

# A model for synaptic development regulated by NMDA receptor subunit expression

Shigeru Kubota · Tatsuo Kitajima

Received: 29 August 2006 / Accepted: 29 March 2007 / Published online: 22 May 2007  
© Springer Science + Business Media, LLC 2007

**Abstract** Activation of NMDA receptors (NMDARs) is highly involved in the potentiation and depression of synaptic transmission. NMDARs comprise NR1 and NR2B subunits in the neonatal forebrain, while the expression of NR2A subunit is increased over time, leading to shortening of NMDAR-mediated synaptic currents. It has been suggested that the developmental switch in the NMDAR subunit composition regulates synaptic plasticity, but its physiological role remains unclear. In this study, we examine the effects of the NMDAR subunit switch on the spike-timing-dependent plasticity and the synaptic weight dynamics and demonstrate that the subunit switch contributes to inducing two consecutive processes—the potentiation of weak synapses and the induction of the competition between them—at an adequately rapid rate. Regulation of NMDAR subunit expression can be considered as a mechanism that promotes rapid and stable growth of immature synapses.

**Keywords** NMDA · Plasticity · STDP · Synaptic competition · Development

## 1 Introduction

NMDA receptors (NMDARs) are cation channels that are gated by the excitatory neurotransmitter glutamate and are

required for the experience-dependent modifications of synaptic circuits (Rema et al. 1998; Daw et al. 1999). Functional NMDARs are heterotetramers formed by the co-expression of the NR1 and NR2 subunits (Stephenson 2001). While the NR1 subunit is expressed throughout, the expression of different NR2 subunits is both spatially and developmentally regulated (Monyer et al. 1994; Sheng et al. 1994). NR2B-containing receptors are predominant in the neonatal forebrain, whereas expression of the NR2A subunit increases with a certain time lag after birth, suggesting a developmental switch in the NMDAR subunit composition. Physiological experiments have shown that the subunit switch depends on the sensory experience during development (Quinlan et al. 1999a,b) and that the decay time of the NMDAR-mediated synaptic current reduces along with a change in the subunit (Flint et al. 1997; Mierau et al. 2004). These findings suggest the possibility that the functional property of NMDARs is controlled via subunit expression depending on the developmental stages.

The decay time of the NMDAR current appears to be critical for the coincidence detection of pre- and postsynaptic events, which is reflected in  $\text{Ca}^{2+}$  increase necessary for synaptic plasticity (Bear et al. 1987). Therefore, it has been hypothesized that the higher ability of plasticity in young animals is correlated with the longer decay time of the NMDAR current (Crair and Malenka 1995; Feldman et al. 1998), and that a reduction in this decay time induces the end of the developmental “critical” period (Fagiolini et al. 1994; Dumas 2005). However, the biophysical mechanisms by which the change in the NMDAR function regulates synaptic development are not fully understood. Thus, in this paper, we consider the effects of the NMDAR subunit switch on early synaptic circuit formation.

---

**Action Editor:** Upinder Bhalla

---

S. Kubota (✉) · T. Kitajima  
Department of Bio-System Engineering, Yamagata University,  
4-3-16 Jonan, Yonezawa, Yamagata 992-8510, Japan  
e-mail: kubota@yz.yamagata-u.ac.jp

Recent experimental results have revealed that synaptic modification depends on the precise timing of pre- and postsynaptic spikes (Markram et al. 1997; Debanne et al. 1998; Bi and Poo 1998; Zhang et al. 1998; Feldman 2000; Nishiyama et al. 2000; Froemke et al. 2005; for review, see Abbott and Nelson 2000), which is termed as spike-timing-dependent plasticity (STDP). In many systems, STDP is characterized by its dependence on the relative timing of the pre- and postsynaptic spikes (Abbott and Nelson 2000); long-term potentiation (LTP) is induced if a presynaptic spike precedes a postsynaptic spike in a short time window, while the reversed spike order induces long-term depression (LTD). Biophysical models of STDP (Kitajima and Hara 2000; Shouval et al. 2002; Karmarkar and Buonomano 2002; Karmarkar et al. 2002; Abarbanel et al. 2003; Rubin et al. 2005) have shown that the timing and order sensitivity of STDP can be largely explained by the standard hypothesis of calcium-dependent plasticity that states that higher levels of  $\text{Ca}^{2+}$  induce LTP, while moderate levels induce LTD (Lisman 1989; Artola and Singer 1993). Therefore, it is possible that the developmental change in the NMDAR kinetics and the resulting change in NMDAR-mediated  $\text{Ca}^{2+}$  signals act as a higher-order plasticity that modulates the time window and strength of STDP.

An important feature of STDP is that it provides a mechanism that forces synapses to compete with each other such that when some synapses to a given postsynaptic cell are strengthened, others are weakened (Song et al. 2000; Rubin et al. 2001). Such a competitive mechanism is particularly important during early development since it is considered to be responsible for input selectivity that is necessary for synaptic organization such as cortical maps (Kepecs et al. 2002). The strong competition between presynaptic inputs also stabilizes the postsynaptic firing rate within a physiological range (Song et al. 2000). These advantages of STDP are based on the property that it potentiates only the presynaptic inputs that frequently contribute to evoking the spike and weakens inputs that cannot contribute to it (Abbott and Nelson 2000). This also indicates a disadvantage of STDP in that it takes a considerably long time for synaptic growth since early synapses are very weak and difficult to evoke a frequent discharge (Issac et al. 1997).

Therefore, in this study, we examine the possibility that the modulation of STDP by the NMDAR subunit switch serves to satisfy both the requirements during early development: the rapid growth of immature synapses and the induction of competition between them. We address two main issues: how the NMDAR subunit switch modifies the STDP learning rule and how the synaptic weight growth is regulated by this change in STDP. To address the first issue, we construct a biophysical model of  $\text{Ca}^{2+}$ -based plasticity and show that the acceleration of the NMDAR decay

mainly suppresses LTP induction in STDP. With regard to the second issue, we examine the synaptic weight dynamics by the Fokker–Planck approach and predict that the NMDAR subunit switch first strengthens each synapse and then introduces competition in order to stabilize the system. We also perform numerical simulations using the integrate-and-fire model to validate the theoretical prediction.

## 2 Methods

### 2.1 Calcium-dependent plasticity model

Here, we construct a model that incorporates the hypothesis of calcium-dependent plasticity (Lisman 1989; Artola and Singer 1993). The basic assumptions of this model are similar to those in Shouval et al. (2002): (1) a change in the synaptic efficacy is determined by the  $\text{Ca}^{2+}$  concentration in the spine (Lisman 1989; Artola and Singer 1993), (2) NMDAR is the major source of  $\text{Ca}^{2+}$  entry into the spine, and (3) the action potential (AP) of a postsynaptic neuron has a slow afterdepolarization (ADP).

The second assumption with respect to the source of  $\text{Ca}^{2+}$  current is based on recent experiments (Kovalchuk et al. 2000; Sabatini et al. 2002). These studies have observed the  $\text{Ca}^{2+}$  signals in dendritic spines of rat CA1 pyramidal neurons during a few postnatal weeks—around the period where the NMDAR subunit switch occurs in this preparation (Kirson et al. 1999). The results have shown that the synaptic  $\text{Ca}^{2+}$  signals are primarily attributable to the  $\text{Ca}^{2+}$  entry through the NMDARs (Kovalchuk et al. 2000); further the synaptically evoked  $\text{Ca}^{2+}$  transient through NMDARs during postsynaptic depolarization is much larger than the single AP-induced  $\text{Ca}^{2+}$  current through voltage-gated calcium channels (VGCCs) (Sabatini et al. 2002). The contribution of intracellular stores to the amplitude of  $\text{Ca}^{2+}$  signals is also small (Kovalchuk et al. 2000; Sabatini et al. 2002). The sources of spine  $\text{Ca}^{2+}$  transients, which are actually involved in the induction of long-term plasticity, continue to be debatable (for review, see Sabatini et al. 2001). However, in addition to the above experimental findings, a theoretical study indicates that the  $\text{Ca}^{2+}$  influx through NMDARs is sufficient to explain the various forms of synaptic plasticity simultaneously (Shouval et al. 2002). Therefore, in the current model, we consider the long-term plasticity induced by NMDAR-mediated  $\text{Ca}^{2+}$  signals.

The third assumption for ADP is required for creating moderate levels of postsynaptic  $\text{Ca}^{2+}$  in order to induce LTD when the presynaptic event follows postsynaptic firing (Shouval et al. 2002; Karmarkar et al. 2002). Slow ADP is a prominent feature of neocortical pyramidal cells (McCormick et al. 1985; Feldman 2000; Froemke et al. 2005) and is also

found in hippocampal pyramidal cells (Callaway and Ross 1995).

We define  $\Delta t = t_{\text{post}} - t_{\text{pre}}$  to be the interspike interval (ISI) between pre- and postsynaptic events;  $\Delta t > 0$  indicates that the postsynaptic spike occurs after the presynaptic spike (pre-post timing), while  $\Delta t < 0$  corresponds to a spike pair in the reverse order (post-pre timing). In conventional STDP models (Kitajima and Hara 2000; Karmarkar et al. 2002), the  $\text{Ca}^{2+}$  peak level  $[Ca]_{\text{peak}}$  is calculated for each ISI from the  $\text{Ca}^{2+}$  time course during the pairing protocol. A change in the synaptic efficacy  $\Delta w$  is then determined such that higher and moderate  $\text{Ca}^{2+}$  peak levels elicit LTP and LTD, respectively (Fig. 1(a), left) (Lisman 1989):

$$\Delta w = f_P([Ca]_{\text{peak}}) + f_D([Ca]_{\text{peak}}). \tag{1}$$

Here,  $f_P(\geq 0)$  and  $f_D(\leq 0)$  are the functions associated with LTP and LTD induction, respectively. This model always induces two disconnected LTD ranges in the pre-post and post-pre timing (Fig. 1(a), right) (Bi and Rubin 2005). This type of STDP curve appears in hippocampal slices (Nishiyama et al. 2000), but it does not agree with the asymmetric time windows (Fig. 1(b), right) observed in other experiments (e.g., Bi and Poo 1998; Feldman 2000;

Froemke et al. 2005). Additionally, there is evidence that the LTD in pre-post timing may be an indirect effect mediated by feedforward GABAergic circuitry (Togashi et al. 2003).

The appearance of two LTD ranges in the conventional model (Eq. (1)) originates from the fact that the calcium time course is converted into just one variable  $[Ca]_{\text{peak}}$ . When  $\Delta t$  moves from  $-\infty$  to  $+\infty$ ,  $[Ca]_{\text{peak}}$  first increases from a base line value to the LTP range and then returns to the base line so that  $[Ca]_{\text{peak}}$  passes the LTD range twice (Fig. 1(a), left). A simple method to overcome this problem is to consider the duration of  $\text{Ca}^{2+}$  elevation. If we define  $T_{Ca}$  as the time interval in which  $[Ca^{2+}]$  is above a threshold  $\sigma_D$ , we can consider a plane spanned by  $[Ca]_{\text{peak}}$  and  $T_{Ca}$ . In this two-variable model, it is possible to produce a closed path that passes the LTD range just once (Fig. 1(b), left) and reproduce a temporal asymmetry in STDP (Fig. 1(b), right).

Actually, there is evidence that the duration of the increase in  $\text{Ca}^{2+}$  affects the plasticity. Physiological experiments have shown that a high  $\text{Ca}^{2+}$  elevation induces LTP even if its duration is short, while a prolonged period of a moderate  $\text{Ca}^{2+}$  increase is required for the stable induction of LTD (Mizuno et al. 2001; Yang et al. 1999). Therefore, we make an assumption that the LTD induction is blocked when the duration of  $\text{Ca}^{2+}$  increase  $T_{Ca}$  is less than a threshold  $\hat{T}$ . If we also assume that  $\hat{T}$  is an increasing function of  $[Ca]_{\text{peak}}$ , the plasticity model can be written as follows:

$$\Delta w = f_P([Ca]_{\text{peak}}) + f_D([Ca]_{\text{peak}}) \cdot f_B(T_{Ca} - \hat{T}([Ca]_{\text{peak}})). \tag{2}$$

Here, the function responsible for the LTD block  $f_B$  is a step function unless otherwise stated:  $f_B(x) = 1$  for  $x > 0$  and  $f_B(x) = 0$  for  $x \leq 0$ . We have assumed that  $\hat{T}$  increases with  $[Ca]_{\text{peak}}$  because a larger  $[Ca]_{\text{peak}}$  generally requires a longer period for  $\text{Ca}^{2+}$  decay and leads to a larger  $T_{Ca}$ . This assumption may be consistent with the action of cAMP-dependent protein kinase that makes the LTD induction difficult for higher  $\text{Ca}^{2+}$  levels (Lisman 1989). The explicit forms of  $f_P$  and  $f_D$  are as follows (Fig. 3(a)):

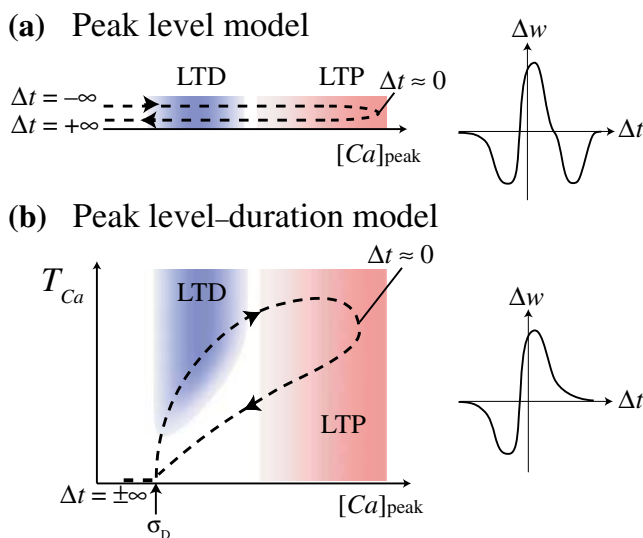


**Fig. 1** The calcium-dependent plasticity model. **(a)** In the conventional model (Eq. (1)) plasticity  $\Delta w$  is determined by the calcium peak level  $[Ca]_{\text{peak}}$  such that LTP and LTD occur at a higher and medium range of  $[Ca]_{\text{peak}}$ , respectively (left). When ISI  $\Delta t$  changes from  $-\infty$  to  $+\infty$ ,  $[Ca]_{\text{peak}}$  first increases and then decreases (left, dashed line); therefore, the LTD range always appears in both positive and negative ISIs (right). **(b)** In the proposed model (Eq. (2)),  $\Delta w$  is given as a function of  $[Ca]_{\text{peak}}$  and  $T_{Ca}$ , where  $T_{Ca}$  is defined as the duration of period that  $[Ca^{2+}]$  is above a threshold  $\sigma_D$ . Hence, it is possible that a set of points ( $[Ca]_{\text{peak}}$ ,  $T_{Ca}$ ) for all ISIs form a closed path such that LTD occurs only once (left, dashed line). In this case, the LTD range appears only for negative ISIs (right). Note that  $T_{Ca}$  converges to 0 when  $[Ca]_{\text{peak}}$  is less than  $\sigma_D$

$$f_P(x) = \begin{cases} \eta_P \left[ -\left( \frac{x - \sigma_M}{\sigma_M - \sigma_P} \right)^2 + 1 \right]^2, & \text{for } x \in (\sigma_P, \sigma_M), \\ 0, & \text{otherwise,} \end{cases} \tag{3}$$

$$f_D(x) = \begin{cases} -\eta_D \left[ -\left( \frac{2x - (\sigma_P + \sigma_D)}{\sigma_P - \sigma_D} \right)^2 + 1 \right]^2, & \text{for } x \in (\sigma_D, \sigma_P), \\ 0, & \text{otherwise.} \end{cases} \tag{4}$$

The maximum levels of LTP and LTD are  $\eta_P=1.3$  and  $\eta_D=1$ , except for Fig. 6(b), where  $\eta_P=0.0085$  and  $\eta_D=0.013$ , respectively. The other parameters are  $\sigma_D=3.5 \mu\text{M}$ ,  $\sigma_P=6 \mu\text{M}$ , and  $\sigma_M=9 \mu\text{M}$ , except for Fig. 4, where  $\sigma_P=5.5$  and  $6.5 \mu\text{M}$  are also used. We simply assume that  $\hat{T}([Ca]_{peak})$  is a linear function:  $\hat{T} = a[Ca]_{peak} + b$  with  $a=14.3 \text{ ms}/\mu\text{M}$  and  $b=-33.2 \text{ ms}$ .

## 2.2 Compartmental model

To simulate the electrophysiological experiments of STDP (e.g., Feldman 2000), we have constructed a compartmental model of a cortical neuron with a simplified pyramidal-cell morphology (Fig. 2(a)). The parameters characterizing the passive dendrites are  $R_m=30 \text{ k}\Omega\text{cm}^2$ ,  $C_m=1 \mu\text{F}/\text{cm}^2$  (membrane time constant  $\tau_m=30 \text{ ms}$ ),  $R_i=300 \Omega\text{cm}$ , and  $E_{leak}=-74 \text{ mV}$  (Koch 1999; Mainen and Sejnowski 1996; Feldman 2000). The soma contains two voltage-dependent currents: fast  $\text{Na}^+$ ,  $I_{Na}$  (with a peak conductance of  $200 \text{ mS}/\text{cm}^2$ ,  $E_{Na}=58 \text{ mV}$ ) and fast  $\text{K}^+$ ,  $I_K$  (with a peak conductance of  $3 \text{ mS}/\text{cm}^2$ ,  $E_K=-80 \text{ mV}$ ). To reproduce the slow ADP observed in pyramidal cells (McCormick et al. 1985; Feldman 2000; Froemke et al. 2005; Callaway and Ross 1995), the peak potassium conductance was decreased to a small value. The simulated waveforms of the AP and the backpropagating AP in the soma and spine are represented by the thin and thick solid lines in Fig. 4(b), respectively. The voltage-gated currents are described by Hodgkin–Huxley-type equations (Mainen and Sejnowski 1996). The input resistance is  $R_{in}=410 \text{ M}\Omega$ , which is within the physiological range for the in vitro recording of neocortical pyramidal cells (Tateno et al. 2004).

Presynaptic inputs to the spine are composed of AMPA receptor (AMPA)- and NMDAR-mediated currents. AMPAR current is described as  $I_{AMPA}=G_A(t)(V-E_A)$ . Its conductance follows an alpha function

$$G_A(t) = \bar{g}_A \cdot \kappa_A \cdot t \exp(-t/t_A), \quad (5)$$

with the peak conductance  $\bar{g}_A = 0.5 \text{ nS}$ ,  $\kappa_A=e/t_A$ ,  $t_A=1.5 \text{ ms}$ , and the reversal potential  $E_A=0 \text{ mV}$  (Zador et al. 1990). The NMDAR current is modeled by incorporating a voltage-dependent  $\text{Mg}^{2+}$  block (Jahr and Stevens 1990a,b; Koch 1999). We represent  $I_{NMDA}=G_N(t)(V-E_N)$ , where

$$G_N(t) = \bar{g}_N \frac{\exp(-t/\tau_1^N) - \exp(-t/\tau_2^N)}{1 + \eta[\text{Mg}] \exp(-\gamma V)}. \quad (6)$$

Here,  $\bar{g}_N$  denotes the peak conductance;  $\tau_1^N$  and  $\tau_2^N$ , the decay and rise time constants, respectively; and  $E_N$ , the reversal potential. The concentration of  $\text{Mg}^{2+}$  ion is  $[\text{Mg}]=1 \text{ mM}$  (Koch 1999). The  $\text{Ca}^{2+}$  current through the NMDAR is represented as  $I_{Ca}=P_f I_{NMDA}$ , where  $P_f$  is the “fractional

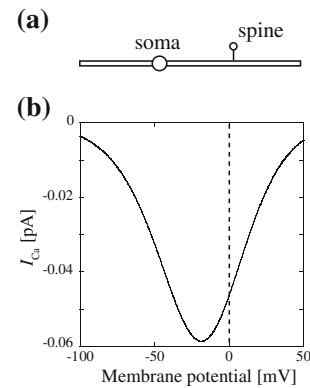


**Fig. 2** A simplified model of a cortical pyramidal neuron. (a) The compartmental model has a spherical soma  $14 \mu\text{m}$  in diameter (1 compartment), an apical dendrite  $4 \mu\text{m}$  in diameter and  $350 \mu\text{m}$  long (7 compartments), a basal dendrite  $4 \mu\text{m}$  in diameter and  $200 \mu\text{m}$  long (4 compartments), and a spine  $2.7 \mu\text{m}^2$  in membrane area (1 compartment). The spine is connected to the center of the apical dendrite with a spine neck resistance of  $41.1 \text{ M}\Omega$ . The size of each dendrite is modified from the model for neocortical pyramidal cells of Bush and Sejnowski (1993), and the shape of the spine is based on the data of Harris et al. (1992). (b) The voltage dependence of the  $\text{Ca}^{2+}$  current through the NMDAR channels (Eq. (7)) with the permeability ratio  $P_{Ca}/P_M=0.6$

$\text{Ca}^{2+}$  current” (Schneggenburger et al. 1993). If we derive  $P_f$  by the method given by Schneggenburger et al., we obtain the following expression:

$$I_{Ca}(t) = G_N(t) \frac{4[\text{Ca}]_o(V - E_N)}{4[\text{Ca}]_o + (P_M/P_{Ca})[\text{M}][1 - \exp(2FV/RT)]}, \quad (7)$$

where  $F$ ,  $R$ , and  $T(=293 \text{ K})$  have their usual meanings, and  $P_M/P_{Ca}$  is the permeability ratio of monovalent ions over  $\text{Ca}^{2+}$  ions. The concentrations of extracellular calcium and monovalent ions are  $[\text{Ca}]_o=1.6 \text{ mM}$  and  $[\text{M}]=155 \text{ mM}$ , respectively (Schneggenburger et al. 1993; Schneggenburger 1996). The voltage dependence of  $I_{Ca}$  is shown in Fig. 2(b).

Calcium in the spine obeys first-order kinetics (Shouval et al. 2002):

$$\frac{d[\text{Ca}]}{dt} = -\frac{[\text{Ca}]}{\tau_s} - \frac{I_{Ca}}{2F \cdot \text{Vol}}, \quad (8)$$

with the time constant  $\tau_s=20 \text{ ms}$  (Sabatini et al. 2002) and the volume of the spine head  $\text{Vol}=0.29 \mu\text{m}^3$  (Harris et al. 1992).

## 2.3 Integrate-and-fire model

To study the modification of the synapses that drive a postsynaptic cell, we use the leaky integrate-and-fire (LIF)

model including  $\text{Ca}^{2+}$ -activated  $\text{K}^+$  current,  $I_{\text{AHP}}$  (Liu and Wang 2001):

$$C \frac{dV}{dt} = g_{\text{leak}}(V_{\text{rest}} - V) - I_{\text{AHP}} + I, \tag{9}$$

$$I_{\text{AHP}} = k[\text{Ca}]_d(V - E_K), \tag{10}$$

$$\frac{d[\text{Ca}]_d}{dt} = -\frac{[\text{Ca}]_d}{\tau_d}. \tag{11}$$

Here, the conductance associated with  $I_{\text{AHP}}$  increases with  $[\text{Ca}]_d$ , the  $\text{Ca}^{2+}$  concentration at a proximal dendrite, which is regulated by the spike-induced entry of  $\text{Ca}^{2+}$  through VGCCs (Lancaster and Zucker 1994; Sah and Bekkers 1996; Svoboda et al. 1997). When the membrane potential reaches a threshold value  $V_{\text{th}}$ , the neuron fires a spike. After firing, the membrane potential is maintained at  $V = V_{\text{reset}}$  during an absolute refractory period  $\tau_{\text{abs}}$ . Each spike also generates a small increase in the  $\text{Ca}^{2+}$  concentration,  $\alpha$ . The parameter values (Table 1) were modified from those of Troyer and Miller (1997) and Liu and Wang (2001). Note that the properties of the dendritic  $\text{Ca}^{2+}$  transients in this model, such as the decay time constant or the effect of single spikes on the  $\text{Ca}^{2+}$  increase, differ from those of the spine  $\text{Ca}^{2+}$  signals in the compartmental model. This is mainly because the difference in the surface-to-volume ratio significantly affects the  $\text{Ca}^{2+}$  transient (Schiller et al. 1995; Helmchen et al. 1996).

The neuron receives inputs from 4,000 excitatory and 800 inhibitory synapses. Each excitatory and inhibitory synapse is activated by independent Poisson spike trains of 3 Hz. If a low success rate (~10%) of the synaptic transmission in developing neurons (Hessler et al. 1993) is considered, this input rate corresponds to the presynaptic firing rate of approximately 30 Hz, which is within the physiological range of the sensory-evoked response of neocortical cells

**Table 1** Parameters for LIF model

Parameter	Value
Membrane capacitance $C$	0.5 nF
Leak conductance $g_{\text{leak}}$	25 nS
Resting potential $V_{\text{rest}}$	-74 mV
Firing threshold $V_{\text{th}}$	-54 mV
Refractory period $\tau_{\text{abs}}$	1.8 ms
Reset potential $V_{\text{reset}}$	-60 mV
$\tau_d$	200 ms
$\alpha$	0.2 $\mu\text{M}$
$k$	12.5 mS/M
Reversal potential $E_K$	-80 mV

$\tau_d$ , time constant for calcium dynamics;  $\alpha$ , calcium increase per action potential;  $k$ , coefficient of the conductance for  $I_{\text{AHP}}$ .

(Ahmed et al. 1998; Simons and Carvell 1989; Simons 1978). The excitatory inputs are evoked by AMPAR and NMDAR conductances given in Eqs. (5) and (6), respectively, while the inhibitory inputs are mediated by the GABA-type conductance  $G_G(t) = \bar{g}_G \cdot \kappa_G \cdot t \exp(-t/t_G)$  with  $\bar{g}_G = 1$  nS,  $\kappa_G = e/t_G$ ,  $t_G = 10$  ms, and an associated reversal potential of -70 mV (Bernander et al. 1991). The currents evoked by past presynaptic inputs are linearly summed for calculating the synaptic current at the present instant.

STDP acts on the excitatory synapses with the additive update rule (Kepecs et al. 2002); in other words, the weight changes are independent of the present weight. All the weights are initially set to  $w(0) = 0.25$ . When a pre- or postsynaptic event occurs, the synaptic weight is updated stepwise by a small amount  $\Delta w$ , which is given by the STDP curve, similar to other studies (Song et al. 2000; Gerstner and Kistler 2002). The updating has been restricted within  $[0, w_{\text{max}}]$  ( $w_{\text{max}} = 2.5$ ). The peak AMPAR conductance is multiplied by the synaptic weight  $w(t)$ .

The deviation of the synaptic weight distribution from its steady state is expressed as  $D_w = \sum_i |N_i - N_i^{SS}| / 2N$ . Here,  $N_i$  is the number of excitatory synapses with the weight  $w$  satisfying  $0.05(i-1) < w/w_{\text{max}} < 0.05i$ ;  $N_i^{SS}$ , the value of  $N_i$  at the steady state; and  $N$ , the total number of excitatory synapses. The time for convergence to the steady state was calculated from the convergence criterion  $D_w < 0.1$ .

### 2.4 Numerical simulation

All models were implemented in the C programming language and integrated using the fourth-order Runge–Kutta method (Press et al. 1988) with a time step size of 0.002 ms for the compartmental simulation and the Euler method with a time step size of 0.02 ms for the LIF simulation. Simulations were performed on a 3 GHz personal computer. The source codes are available upon request.

## 3 Results

### 3.1 Developmental change in STDP curve

We performed simulations using a compartmental model (Fig. 2(a)) to study the developmental change in the STDP learning. In order to examine the effects of the NMDAR subunit switch, we performed the simulations with two different parameters for the NMDAR conductance model (Eq. (6)): in the “early” model before the subunit switch, the decay time constant is  $\tau_1^N = 139$  ms, while it is reduced

to  $\tau_1^N = 89$  ms in the “late” model after the subunit switch (Table 2) (Mierau et al. 2004). Experimental findings indicate that the peak amplitude of NMDAR-mediated synaptic currents does not change when their decay time course accelerates during development (Carmignoto and Vicini 1992; Shi et al. 1997; Steigerwald et al. 2000). An experiment with the transfection of NMDAR subunits also suggests that the subunit composition does not alter the amplitude of NMDAR-mediated synaptic currents, probably due to the regulatory mechanism that controls the amount of NMDARs at functional synaptic sites (Prybylowski et al. 2002). Furthermore, there exists evidence that the rise time (Carmignoto and Vicini 1992), voltage dependency (Feldman et al. 1998; Kuner and Schoepfer 1996; Monyer et al. 1994; but see Kato and Yoshimura 1993), and calcium permeability (Schneppenburger 1996) of the NMDAR current are not significantly affected by the developmental change in the subunit composition. Therefore, the parameters other than the decay time constant were set to the same values for the two NMDAR conductance models (Table 2).

To simulate the pairing protocol, a presynaptic input was paired with a brief somatic current injection. After calculating the  $\text{Ca}^{2+}$  time course in the spine for each ISI, we applied the calcium-dependent plasticity model given by Eq. (2). As expected, a slower NMDAR decay contributes to the accumulation of  $\text{Ca}^{2+}$ , and thus, the  $\text{Ca}^{2+}$  peak level for the “early” model is larger than that for the “late” model at all ISIs (Fig. 3(b)). However, the difference between the two models (Fig. 3(b), dashed line) is considerably larger in the pre-post timing. This is because a higher NMDAR conductance remains available in the “early” condition for a relatively long time after a presynaptic input and the backpropagating AP in the pre-post timing triggers a pronounced surge of  $\text{Ca}^{2+}$  (Fig. 3(c), black dashed line). Note that  $[Ca]_{\text{peak}}$  becomes constant for

sufficiently large positive ISIs in Fig. 3(b), since the  $\text{Ca}^{2+}$  increase by the spike is too small to exceed that given by the presynaptic input alone.

The LTD block mechanism implemented by the step function  $f_B$  (Eq. (2)) suppresses the LTD induction in the pre-post timing in the following manner. The rapid voltage change in the early phase of the AP affects the  $\text{Ca}^{2+}$  time course only when the postsynaptic AP occurs after the presynaptic input, i.e., in the pre-post timing. Thus, the duration  $T_{Ca}$ , which is the time interval for which  $[Ca^{2+}]$  is above the threshold, is shorter for the pre-post timing than for the post-pre timing when the same  $\text{Ca}^{2+}$  peak level is attained. Thus, a set of points ( $[Ca]_{\text{peak}}, T_{Ca}$ ) for all ISIs generates a closed path in which  $T_{Ca}$  takes smaller values for positive ISIs (Fig. 3(d)). In our model, LTD is suppressed when  $T_{Ca}$  is less than  $\hat{T}$  (Eq. (2)). Therefore, by setting the function  $\hat{T}([Ca]_{\text{peak}})$  such that it lies between the paths for the positive and negative ISIs, as shown in Fig. 3(d) (blue dotted line), the LTD induction for the pre-post timing is completely blocked while maintaining LTD for the post-pre timing (Fig. 3(e), solid lines). Additionally, the LTD block functions effectively even if  $f_B$  is a more realistic continuous function:  $f_B(x) = 1/[1 + \exp(-x/2)]$  (Fig. 3(e), dotted lines).

The sign of the integral of the STDP curve plays an important role in the stability of the synaptic weight dynamics (Song et al. 2000). Therefore, we have examined the areas of the STDP curve under the LTP and LTD portions— $S_+ = \int_{f>0} f(x)dx$  and  $S_- = -\int_{f<0} f(x)dx$ —and their ratio  $S_-/S_+$  as functions of the NMDAR decay time constant (Fig. 4). It appears that  $S_-/S_+$  depends significantly on how each  $\text{Ca}^{2+}$  level is assigned to the LTP or LTD range. Therefore, we used three sets of functions  $f_P$  and  $f_D$  (Eqs. (3) and (4)) in Fig. 4(a). Additionally, in order to confirm that the results are not dependent on the detailed cell morphology or the AP waveform, we performed the same simulations with the backpropagating AP expressed as the sum of two exponentials (Fig. 4(b), dashed lines; Shouval et al. 2002):

$$V_{AP}(t) = A_{AP} \times [a_f \exp(-t/\tau_f) + a_{ADP} \exp(-t/\tau_{ADP})] + V_{\text{rest}}. \quad (12)$$

Figure 4(c–f) show the changes in  $S_+$ ,  $S_-$ , and  $S_-/S_+$  for the simulations using the compartmental model (Fig. 4(c and d)) and the analytical form of AP in Eq. (12) (Fig. 4(e and f)). Here, each value has been normalized to that of the “early” condition since the absolute quantities depend on the scale of LTP and LTD and are not so meaningful. The figures indicate that a faster NMDAR kinetics decreases  $S_+$  more than  $S_-$  (Fig. 4(c and e)), leading to an increase in  $S_-/S_+$  (Fig. 4(d and f)) independent of the details of the

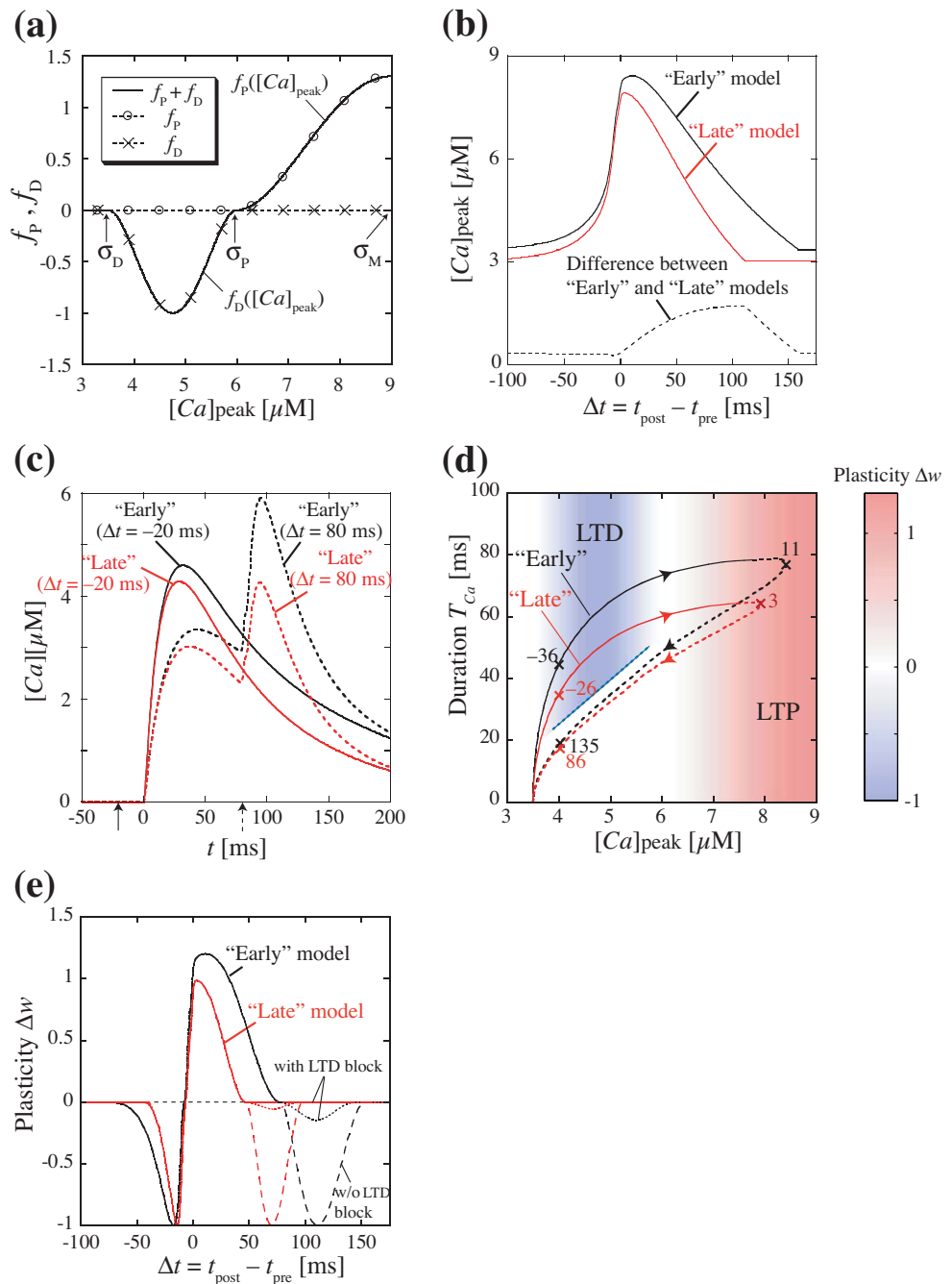
**Table 2** Parameters for NMDAR conductances in the “early” and “late” models

Parameter	“Early” (compartmental/LIF model)	“Late”
$\tau_1^N$ (ms)	139	89
$\tau_2^N$ (ms)	0.67	–
$\bar{g}_N$ (nS)	0.2/0.128	0.2
$\eta$ (/mM)	0.33	–
$\gamma$ (/mV)	0.06	–
$P_{Ca}/P_M$	0.6	–

$\tau_1^N$ , decay time constant;  $\tau_2^N$ , rise time constant;  $\bar{g}_N$ , peak conductance;  $\eta$  and  $\gamma$ , coefficients representing voltage dependence;  $P_{Ca}/P_M$ , permeability ratio between  $\text{Ca}^{2+}$  and monovalent ions. The notation ‘–’ implies that identical values are used in the “early” and “late” models.

**Fig. 3** Predicted outcomes of the compartmental simulations.

(a) The functions  $f_P$  and  $f_D$  in Eqs. (3) and (4). (b)  $[Ca]_{peak}$  vs. ISI relationship for the “early” (black) and “late” (red) models. The dashed line denotes the difference between the two models. (c) Calcium time course when a presynaptic input is paired with a postsynaptic firing for  $\Delta t = -20$  ms (solid) and 80 ms (dashed). Black and red lines correspond to the “early” and “late” NMDAR models, respectively. The arrows denote spike timing for the two ISIs. (d) Duration  $T_{Ca}$ , the time interval for which  $Ca^{2+}$  is above a threshold, is plotted vs.  $[Ca]_{peak}$  for each ISI (similar to Fig. 1(b)) with the “early” (black) and “late” (red) models. The solid and dashed lines denote negative and positive ISIs, respectively. Each number denotes the value of the corresponding ISI. Background color shows values of plasticity  $\Delta w$  for each point ( $[Ca]_{peak}$ ,  $T_{Ca}$ ). Blue dotted line shows the lower limit of  $T_{Ca}$  for LTD induction ( $\hat{T}$ ), which is a function of  $[Ca]_{peak}$ . (e) The STDP curves for the “early” (black) and “late” (red) models. Solid lines represent cases where  $f_B$  in Eq. (2) is the step function, while dotted lines represent cases where  $f_B(x) = 1/[1 + \exp(-x/2)]$ . Dashed lines indicate the results of the conventional plasticity model (Eq. (1)) for comparison

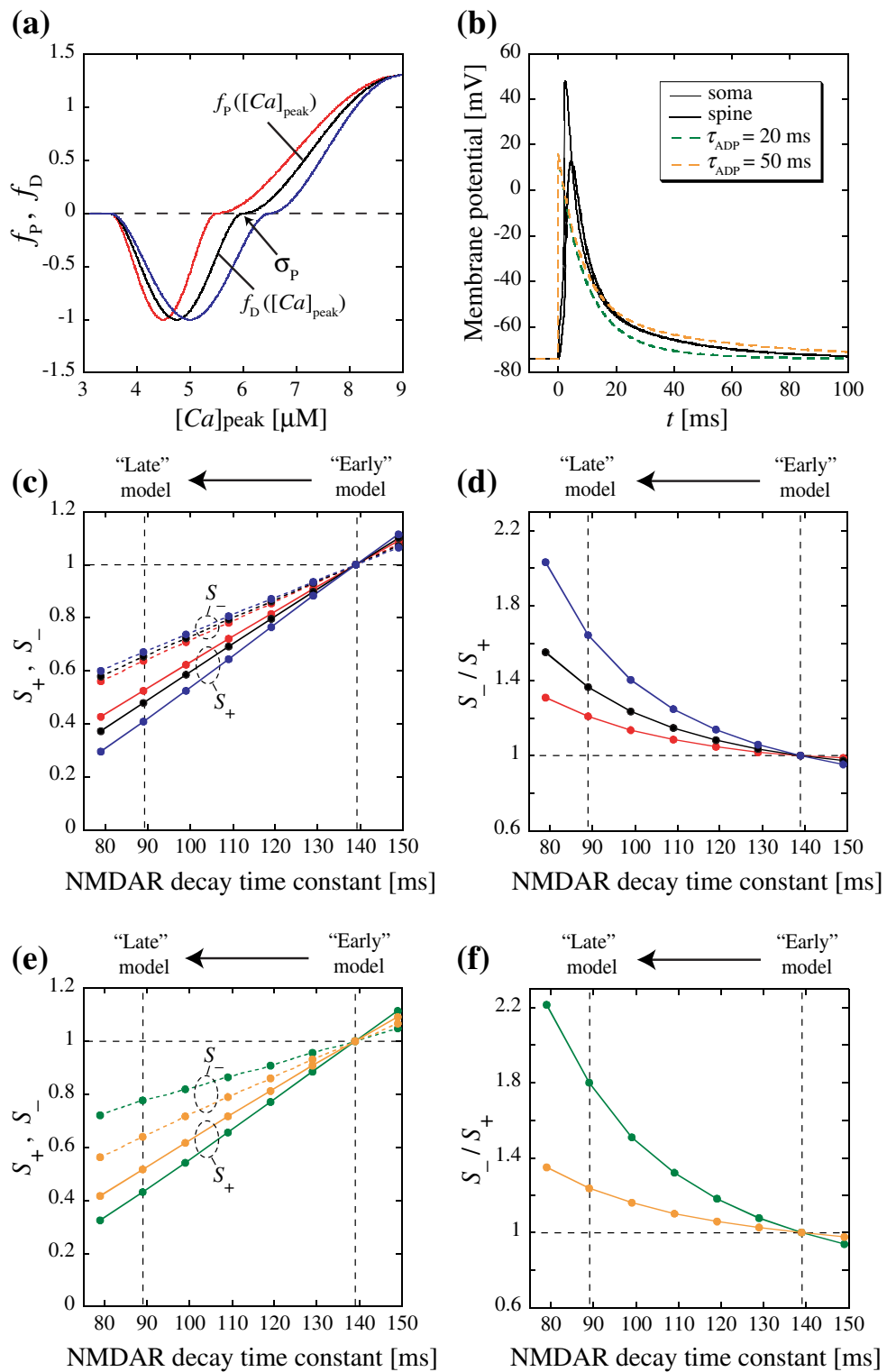


model. These results show that the primary effect of the developmental change in the NMDAR kinetics is to suppress the degree of LTP, which leads to an increase in the relative effects of LTD compared to those of LTP.

Previous calcium-based plasticity models also have examined the effects of the NMDAR kinetics on the STDP curve (Shouval et al. 2002, Fig. 5; Karmarkar and Buonomano 2002, Fig. 2). These models significantly differ from ours on the point that the LTD range appears for both the pre-post and post-pre timing, as shown in

Fig. 1(a) (right). However, our results and theirs are similar in that a faster NMDAR kinetics tends to inhibit LTP significantly in the pre-post timing. The higher sensitivity of LTP to the NMDAR kinetics is based on a simple mechanism that the change in the NMDAR decay primarily influences the spike-induced  $Ca^{2+}$  influx during the decay phase, i.e., in the pre-post timing (Fig. 3(b and c)). Therefore, similar results can be obtained for a relatively wide variety of models or model parameters (Fig. 4), as long as the magnitude of LTP is continuously changed with the  $Ca^{2+}$  level.

**Fig. 4** The NMDAR subunit switch modifies the STDP curve such that the areas under the LTP portion ( $S_+$ ) and the LTD portion ( $S_-$ ) decrease, while their ratio ( $S_-/S_+$ ) increases. **(a)** The functions  $f_P$  and  $f_D$  in Eqs. (3) and (4). Since the ratio  $S_-/S_+$  depends significantly on how each  $Ca^{2+}$  level is assigned to the LTP or LTD range, we used three different values for the  $Ca^{2+}$  concentration of the LTP threshold  $\sigma_P$ :  $\sigma_P=5.5$  (red), 6 (black; identical to Fig. 3(a)), and  $6.5 \mu M$  (blue). **(b)** The AP waveforms obtained by the compartmental simulations (solid lines) and the sum of exponential functions (Eq. (12); dashed lines) with  $A_{AP}=90$  mV,  $a_f=0.75$ ,  $a_{ADP}=0.25$ ,  $\tau_f=8$  ms,  $V_{rest}=-74$  mV, and  $\tau_{ADP}=20$  ms (green) or 50 ms (orange). **(c)** and **(d)**  $S_+$  and  $S_-$  (e), and their ratio  $S_-/S_+$  (d) are plotted with the NMDAR decay time constant. These values are obtained by simulations using the compartmental model and are normalized to those for the “early” model. For each plot, the functions  $f_P$  and  $f_D$  are in the same color in (a). **(e)** and **(f)** The results similar to (c) and (d), except that backpropagating AP is represented by the sum of exponential functions (Eq. (12)). For each plot, the shape of the backpropagating AP is in the same color in (b). (Functions  $f_P$  and  $f_D$  are the same as the black curve in (a).)



### 3.2 Theoretical prediction by Fokker–Planck approach

If the NMDAR subunit switch acts to modify the STDP curve, as shown in the above simulations, how does this change regulate synaptic growth? Here, we theoretically

examine the effects of the change in the STDP curve on the synaptic weight dynamics. Some experiments suggest that the change in the NMDAR subunit composition can be triggered by an increase in the neuronal activity quite rapidly (Quinlan et al. 1999a,b; Philpot et al. 2001; Carmignoto and

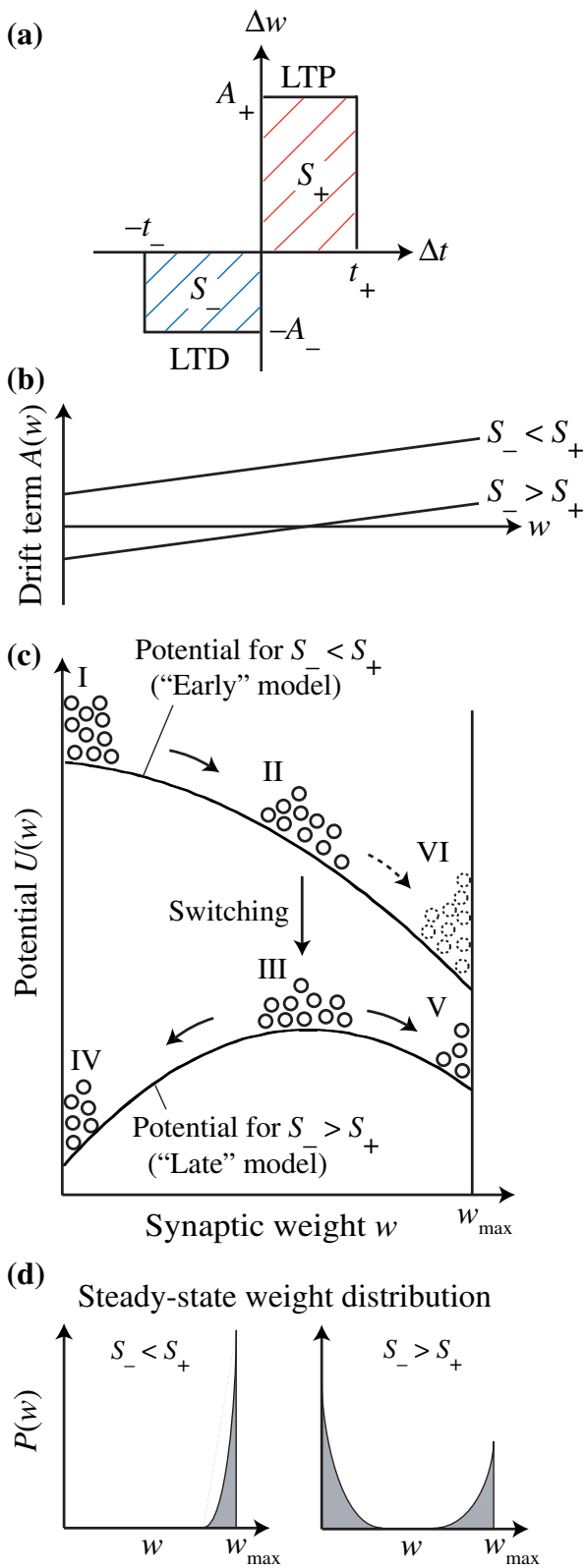


**Fig. 5** Theoretical prediction by the Fokker–Planck approach. (a) A simplified STDP curve.  $S_+ = A_+ t_+$  and  $S_- = A_- t_-$  indicate the areas under the LTP and LTD portions, respectively. (b) Schematic illustrations of the drift term  $A(w)$  for two cases: (1)  $S_- < S_+$ , and (2)  $1 < S_- < S_+ < 1 + w_{max}/W_{tot}$  (labeled as  $S_- > S_+$ ). (c) The predicted effects of the NMDAR subunit switch on the temporal evolution of synaptic weights. The two *solid curves* show the potential  $U(w) = -\int_0^w A(w')dw'$  corresponding to  $A(w)$  in (b). The *solid circles* in states I–V and the *solid arrows* illustrate the synaptic weight change regulated by the NMDAR subunit switch. First, initially weak synapses (state I) are strengthened (state II). After the subunit switch occurs (state III), the synapses converge to the bimodal weight distribution (states IV and V) by going down the potential. The *dashed circles* (state VI) and *dashed arrow* indicate a case of delayed switching. (d) Steady-state weight distribution predicted by the potential in (c)

Van Rossum et al. (2000) have shown that when many presynaptic inputs randomly drive a postsynaptic cell, the temporal evolution of the synaptic weights is described by the Fokker–Planck equation. If we apply their method to the STDP curve with  $\Delta w = A_+$  for  $0 < \Delta t < t_+$  and  $\Delta w = -A_-$  for  $-t_- < \Delta t < 0$  (Fig. 5(a)), the dynamics of the weight distribution  $P(w)$  is represented as follows (Appendix A):

$$\frac{1}{f_{pre} f_{post}} \frac{\partial P(w, t)}{\partial t} = -\frac{\partial}{\partial w} [A(w)P(w, t)] + \frac{1}{2} \frac{\partial^2}{\partial w^2} [B(w)P(w, t)], \quad (13)$$

$$A(w) = S_+(1 - S_-/S_+ + w/W_{tot}), \quad (14)$$

$$B(w) = A_+ S_+(1 + A_- S_- / A_+ S_+ + w/W_{tot}). \quad (15)$$

Here, we have assumed that the weight updating is additive, i.e., the magnitude of weight change is independent of the synaptic strength (Kepecs et al. 2002).  $f_{pre}$  and  $f_{post}$  denote the pre- and postsynaptic rates;  $S_+ = A_+ t_+$  and  $S_- = A_- t_-$ , the areas of the STDP curve under the LTP and LTD portions, respectively; and  $W_{tot} = t_+ f_{pre} n \langle w \rangle$ , the competition parameter for  $n$  excitatory synapses (van Rossum et al. 2000). The drift term  $A(w)$  has a role similar to the average force, and a synapse for a given weight  $w$  increases or decreases depending on whether  $A(w)$  is positive or negative (Risken 1989; Kepecs et al. 2002). Thus, if we define a potential  $U(w) = -\int_0^w A(w')dw'$  (Kepecs et al. 2002), the average motion of the synapses is determined by the gradient of the potential.

The behavior of the synaptic weights depends greatly on which among  $S_+$  and  $S_-$  is greater. When  $S_- < S_+$ ,  $A(w)$  satisfies  $A(0) > 0$  and  $\partial A(w)/\partial w > 0$ . Therefore,  $A(w)$  is always positive (Fig. 5(b)), and the potential  $U(w)$  monotonically decreases with increasing  $w$  (Fig. 5(c)). Hence, if an upper limit on the synaptic weight,  $w_{max}$ , is imposed, each synapse is pushed toward the limit, and the

Vicini 1992). Therefore, in the following analysis, we simply assume that the subunit switch occurs instantaneously when the synaptic activity matures to a certain level.

final weight distribution clusters near  $w_{\max}$  (Fig. 5(d), left). On the other hand, if  $S_-$  is slightly greater than  $S_+$  such that  $1 < S_-/S_+ < 1 + w_{\max}/W_{\text{tot}}$ ,  $A(0) < 0$  and  $A(w_{\max}) > 0$  hold. This implies that  $A(w)$  changes from negative to positive values with increasing  $w$  (Fig. 5(b)) so that  $U(w)$  takes a peak value at  $w$  satisfying  $A(w) = 0$  (Fig. 5(c)). Therefore, the steady-state weight distribution is bimodal with two clusters around  $w = 0$  and  $w_{\max}$  (Fig. 5(d), right).

An STDP model that results in a bimodal weight distribution has two significant features—synaptic competition and firing rate stabilization (Kepecs et al. 2002). These properties are particularly important for early development. The synaptic competition underlies a mechanism by which a cell acquires selectivity to specific aspects of its inputs and is necessary for the formation of cortical maps. Moreover, the number of synapses per cortical cell increases by more than ten-fold during the first few postnatal weeks (Micheva and Beaulieu 1996); therefore, it is important to stabilize the firing activity by developmentally regulating the total excitatory inputs.

However, the potential for  $S_- > S_+$  depicted in Fig. 5(c) also indicates a defect in that the system takes a long time to converge to the bimodal distribution. Since each synapse is initially very weak in early development (Issac et al. 1997), some synapses must be increased from  $w \approx 0$  to reach the bimodal distribution. However, this process is very slow since these synapses have to climb over the potential. We have shown the possibility that the NMDAR subunit switch modifies the STDP curve such that the ratio of the area under the LTD portion to that under the LTP portion ( $S_-/S_+$ ) increases (Fig. 4). Let us consider that this change leads to a transition of the potentials in Fig. 5(c) from the state of  $S_- < S_+$  to  $S_- > S_+$ . Initially, the potential for  $S_- < S_+$  plays a role in increasing all the synapses toward  $w_{\max}$ . Hence, the synaptic weights increase rapidly from state I, which is denoted by the open circles in Fig. 5(c). If the potential is switched when the synapses reach state II, the system transforms into state III, where the synapses cluster around the peak of the potential for  $S_- > S_+$ . After switching, the synapses can split into two groups and travel down the potential either to the state around  $w = 0$  (state IV) or to the state near  $w_{\max}$  (state V). Therefore, we predict that the NMDAR subunit switch will enable the system to rapidly converge to the bimodal distribution without the slow process of climbing up the potential.

It should be noted that the discussion here also predicts the existence of an “optimal” switch timing that enables the fastest convergence to the bimodal weight distribution. Consider that the system starts from state I in Fig. 5(c). If the potential switch is delayed, the system passes over state II and comes close to state VI (dotted circles), where the synaptic weights are much larger than those in state II. After switching the potential, some synapses must decrease

by climbing over the potential for  $S_- > S_+$  in order to attain bimodal distribution. Thus, a delay in switching will lead to slower convergence.

The key assumption in this theory is that  $S_-$  becomes slightly larger than  $S_+$  after the subunit switch. In the discussion, we consider the possibility that causes this balanced state.

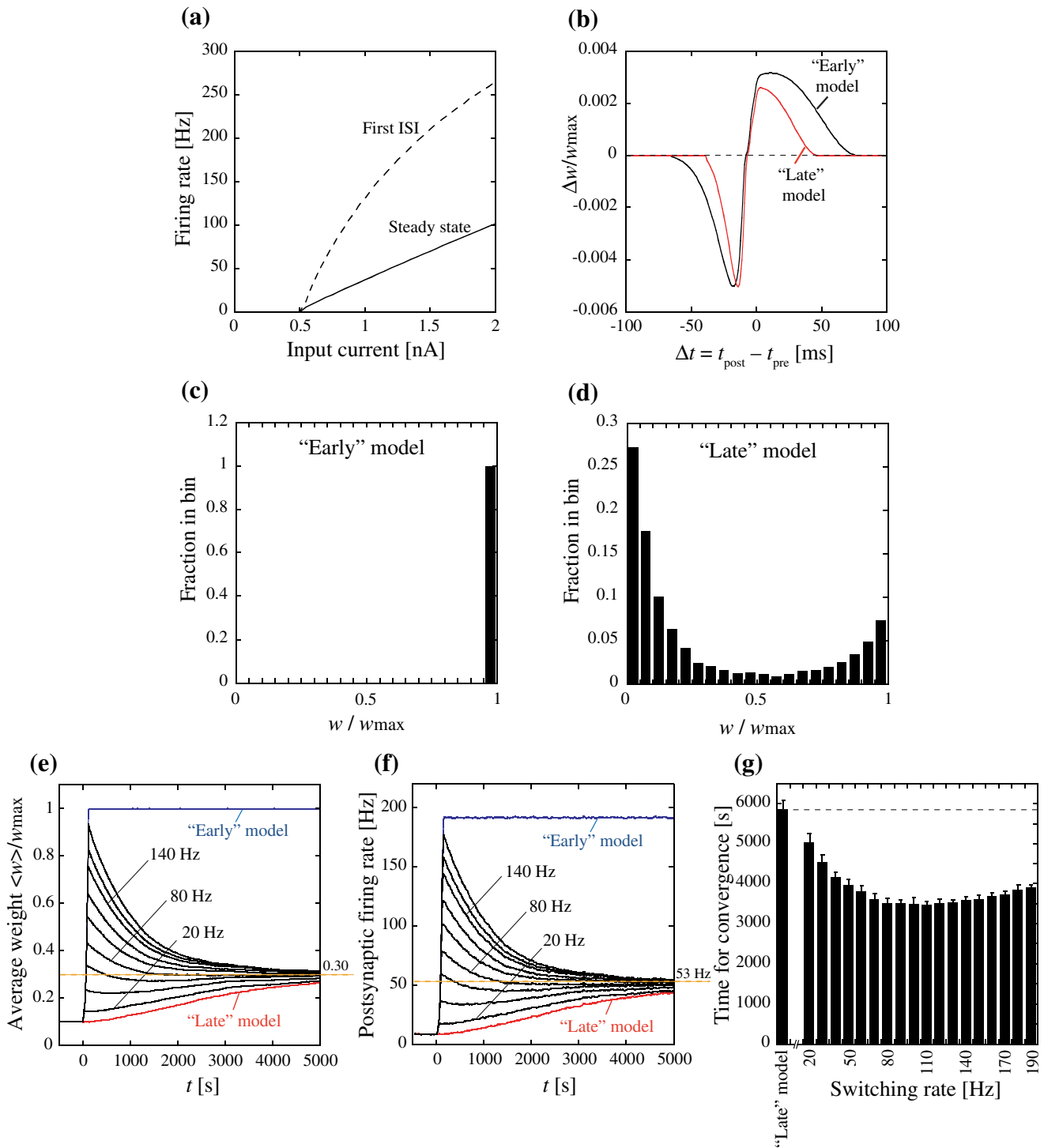
### 3.3 Synaptic weight dynamics regulated by NMDAR subunit switch

To examine the validity of the theoretical prediction, we performed a numerical simulation of the synaptic weight dynamics. We used the LIF neuron model including  $I_{\text{AHP}}$  (Liu and Wang 2001) to reproduce the physiological neuronal gain with lower computational costs. The initial as well as the steady-state  $f-I$  curves are shown in Fig. 6(a), which are comparable to the data of in vivo recordings of neocortical cells (Ahmed et al. 1998). The neuron receives random inputs from excitatory and inhibitory synapses, and the strength of the excitatory synapses is modified by the STDP rule. The number of excitatory and inhibitory synapses (4,000 and 800, respectively) was chosen such that it closely agrees with the data of the rat somatosensory cortex on postnatal day 15 (Micheva and Beaulieu 1996),

**Fig. 6** The results of the simulations using the LIF neuron model. **(a)** The  $f-I$  relationship of the model neuron is similar to that of in vivo neocortical cells (Ahmed et al. 1998). The instantaneous spike frequency for the first spike interval and the steady-state discharge frequency are denoted by the *dashed* and *solid* lines, respectively. **(b)** The STDP curves used in the LIF simulations for the “early” (*black*) and “late” (*red*) models. Two curves were obtained by the simulations using the compartmental model (similar to Fig. 3(e)). The magnitude of the STDP curve  $|\Delta w/w_{\max}|$  is up to  $\sim 0.003$  and  $\sim 0.005$  for the potentiation and depression, respectively (the maximum weight  $w_{\max} = 2.5$ ). These values correspond to the relative weight changes of  $\sim 45\%$  and  $\sim 75\%$  for the synapses with weight size  $w = 1$ , when 60 pairs of pre- and postsynaptic spikes occur repeatedly as in the case of the physiological experiment (Froemke et al. 2005). **(c)** and **(d)** Steady-state weight distribution when the “early” (**c**) or “late” (**d**) model is used. **(e)** and **(f)** Time course of average synaptic weight (**e**) and postsynaptic firing rate (**f**). *Black lines* show the cases where switching from the “early” to “late” model occurs when the postsynaptic rate reaches a given value (switching rate). The switching rate changes by 20 Hz between 20 and 180 Hz, as shown by the labels. The *blue* and *red lines* represent the cases where either the “early” (*blue*) or “late” (*red*) model is used throughout. The *horizontal dashed lines* indicate the steady-state values. **(g)** The time taken for convergence to the steady-state bimodal weight distribution shown in **(d)**. Data shown are the mean and standard deviation of the convergence time for eight simulations using different Poisson trains of inputs. The *leftmost bar* represents the convergence time when the “late” model is used without switching, and the other bars represent the cases where the NMDAR subunit switch occurs at various switching rates. The difference between the convergence time for each switching rate and that for no switching (*horizontal line*) represents the reduction of the convergence time by the NMDAR subunit switch

which is around the period during which the NMDAR subunit switch occurs in this brain area (Mierau et al. 2004). In order to incorporate the effects of the NMDAR subunit switch on STDP, we used two STDP curves corresponding to the “early” and “late” models obtained by the compartmental simulations (Fig. 6(b)). The ratio  $S_-/S_+$  is 0.75 for the

“early” model and 1.02 for the “late” model, which agree with the assumption in the theory. For the input frequency in the current simulation (3 Hz), it appears that the charge transfer mediated by the NMDAR current does not change significantly by the subunit switch because of a slower recovery from the desensitization of the NR2B-containing



receptors (Erreger et al. 2005, Vicini et al. 1998). Hence, the peak conductance of the “early” NMDAR model was decreased such that its charge transfer matches that of the “late” model (Table 2). The steady-state weight distributions obtained by the “early” and “late” models are shown in Fig. 6(c and d). The final distribution of the “early” model clusters near the upper limit (Fig. 6(c)), while that for the “late” model is bimodal (Fig. 6(d)). These results are consistent with the theory (Fig. 5(d)).

We then examined how the NMDAR subunit switch affects the transient response of the system. As mentioned above, some experiments suggest that the change in the NMDAR subunit composition can be rapidly induced by the increase in neuronal activity (Quinlan et al. 1999a,b; Philpot et al. 2001; Carmignoto and Vicini 1992). Therefore, the properties of both the NMDAR conductance (Table 2) and the STDP curve (Fig. 6(b)) were changed from the “early” to “late” model at the moment the postsynaptic firing rate attains a given value, which we refer to as the switching rate. The time for convergence to the steady-state bimodal distribution was measured for various switching rates (Fig. 6(g)) (see Section 2).

Figure 6(e and f) show the time course of the average synaptic weight and the postsynaptic firing rate for different switching rates. The synapses are potentiated much faster with the “early” model than with the “late” model (Fig. 6(e)). Therefore, by switching the model after the synapses are strengthened, the time for convergence to the bimodal weight distribution is significantly shortened, as shown in Fig. 6(g). The figure also indicates the existence of an optimal switching rate (approximately 110 Hz) that enables the fastest convergence. These results agree with the theoretical prediction. An additional set of simulations were carried out by fixing the NMDAR conductance model to either the “early” or “late” condition and switching only the STDP curve. Also in this case, similar results were obtained (data not shown). Hence, the results here are mainly attributable to the effects of switching the STDP curve, as predicted by the theory.

It should be noted that even when the switching rate is greater than the optimal rate, an increase in the convergence time from its minimum is small (Fig. 6(g)). This is because the delay in switching increases the average postsynaptic rate (Fig. 6(f)) and increases the total number of pre- and postsynaptic spike pairs that elicit STDP. The effect can also be understood from the fact that the inverse of the product of the pre- and postsynaptic rates becomes the time constant of the Fokker–Planck equation (Eq. (13)). Therefore, a small delay in the switch timing would not have a strong influence on the convergence time. This appears to suggest that the NMDAR subunit switch induces rapid convergence to the bimodal distribution without precise control of the switch timing.

## 4 Discussion

In this study, we explored the effects of the developmental change in the NMDAR subunit expression on the STDP curve and the synaptic weight dynamics. Our results suggest the following hypothesis to explain the possible roles of the subunit switch. The acceleration of the NMDAR decay attenuates  $\text{Ca}^{2+}$  influx to the spine when a presynaptic event is paired with postsynaptic firing (Fig. 3(b)). Since this effect is much more prominent at positive ISIs than at negative ISIs (Fig. 3(b), dashed line), the NMDAR subunit switch decreases the overall effects of LTP more than those of LTD, leading to an increase in the LTD/LTP ratio (Fig. 4(c–f)). Prior to the subunit switch, LTP exceeds LTD. This contributes to the potentiation of all the synapses (Fig. 5(c)), which are initially very weak during early development (Issac et al. 1997). After the switch, LTD slightly exceeds LTP, inducing competition among different synapses quite rapidly (Figs. 5(c) and 6(g)). Synaptic competition is very important for early synaptic organization as well as the stabilization of neuronal activity (Kepecs et al. 2002; Song et al. 2000). However, competition involves the potentiation of strong synapses and depression of weak synapses, and thus, it inhibits the growth of the initially weak synapses. Therefore, the modulation of the STDP learning rule by the NMDAR subunit expression is required to fulfill the two conflicting requirements—potentiation of immature synapses and induction of competition between them—at an adequately rapid rate.

The LIF neuron model used for examining the prediction by the Fokker–Planck analysis can reproduce a firing rate gain similar to that of neocortical cells, as mentioned above (Fig. 6(a)). However, this model still ignores the mechanism of spike generation by voltage-dependent  $\text{Na}^+$  and  $\text{K}^+$  conductances, which are incorporated in the compartmental model used for examining the change in the STDP curve. Although the voltage-gated conductances may have important effects on the firing behavior (Llinas 1988), we consider that the results of the LIF simulation (Fig. 6) do not significantly depend on the output cell dynamics. The general theoretical analysis of Rubin et al. (2001) indicates that independent of the details of the firing dynamics, the additive STDP model (Kepecs et al. 2002) that has a bias towards LTP elicits the positive drift of the synapses, while the STDP model that has a weak bias towards LTD induces the positive and negative drift for the strong and weak synapses, respectively, as shown in Fig. 5(b). Therefore, the transition from the former to the latter STDP model will yield faster convergence to the bimodal weight distribution, as shown in the schematic diagram in Fig. 5(c). The argument here is also supported by the recent studies that have revealed that STDP can induce synaptic competition

in the compartmental neuron that contains voltage-gated  $\text{Na}^+/\text{K}^+$  currents in the soma and dendrites (Iannella and Tanaka 2006; Rumsey and Abbott 2006).

#### 4.1 $\text{Ca}^{2+}$ -dependent plasticity model

The plasticity model that determines the synaptic modifications solely from the amplitude of  $\text{Ca}^{2+}$  signals induces LTD in two distinct domains of positive and negative ISIs (Fig. 1(a), right) (Bi and Rubin 2005). This type of STDP curve is observed for hippocampal slices (Nishiyama et al. 2000), but it disagrees with other experimental results that show asymmetric temporal windows (Fig. 1(b), right). Therefore, previous STDP models have considered various factors that prevent pre-post timing LTD, such as the stochasticity in  $\text{Ca}^{2+}$  dynamics (Shouval and Kalantzis 2005), independent chemical pathways activated by  $\text{Ca}^{2+}$  entry through NMDARs and VGCCs (Karmarkar and Buonomano 2002), and the temporal property of  $\text{Ca}^{2+}$  signals (Rubin et al. 2005). Among these, the model of Rubin et al. is closely related to ours, although their mathematical description is quite different. Rubin et al. (2005) have reproduced STDP not only by pre- and postsynaptic spike pairs but also by spike triplets or quadruplets based on three assumptions: (1) LTP is induced by the increase in  $\text{Ca}^{2+}$  above a high threshold; (2) LTD is induced if the period in which  $[\text{Ca}^{2+}]$  is above a low threshold is sufficiently long; and (3) LTD induction is suppressed by the increase in  $\text{Ca}^{2+}$  above a mid-level threshold. Our model used the first two assumptions and also assumed that the minimal duration of  $\text{Ca}^{2+}$  signals for LTD induction ( $\hat{T}$ ) increases with the  $\text{Ca}^{2+}$  peak amplitude. This assumption appears to play a role similar to assumption (3) in the study by Rubin et al. (2005) for making LTD induction hard to occur as the  $\text{Ca}^{2+}$  level increases. The two models consistently indicate that the temporal factors of  $\text{Ca}^{2+}$  signals are sufficient to explain the temporal asymmetry of the STDP curve. As mentioned above, a key result of our model that the NMDAR kinetics affects LTP more than LTD (Fig. 4(c and e)) is due to the sensitivity of the spike-induced  $\text{Ca}^{2+}$  influx to the NMDAR decay process. Therefore, similar results would be obtained independent of the manner in which the pre-post timing LTD is prevented when NMDAR current contributes significantly to the  $\text{Ca}^{2+}$  signal in the spine (Sabatini et al. 2001).

Recently, it has been shown that a  $\text{Ca}^{2+}$ /calmodulin-dependent protein kinase II (CaMKII)-mediated potentiation process and a calcineurin-mediated depression process are activated in STDP (Wang et al. 2005), suggesting that STDP is regulated by the calcium and subsequent kinase and phosphatase pathways in a manner similar to classical LTP and LTD (Lisman 1989, 1994; Blitzer et al. 1998;

Bhalla and Iyengar 1999; Holmes 2000; Zhabotinsky 2000; Lisman and Zhabotinsky 2001; Cavazzini et al. 2005). Although the detailed molecular pathways that lead to STDP are still unclear, we consider that each term in the proposed plasticity model (Eq. (2)) may be correlated with the different signaling pathways that control the kinase and phosphatase activity. The effect of function  $f_P$  is similar to that of the autophosphorylation of CaMKII, which produces LTP at higher  $\text{Ca}^{2+}$  concentrations (Lisman 1989; Holmes 2000; Lisman and Zhabotinsky 2001). The LTD induction and blocking mechanisms incorporated by functions  $f_D$  and  $f_B$  resemble the competing actions of calcineurin and cAMP, which elicit the activation and inactivation of protein phosphatase 1 (PP1), respectively, and control the LTD production depending on the  $\text{Ca}^{2+}$  concentration (Lisman 1989; Bhalla and Iyengar 1999). These signaling pathways are mediated through calmodulin (CaM)-regulated proteins. CaM has four  $\text{Ca}^{2+}$ -binding sites with an average dissociation constant ( $K_d$ ) of  $\sim 15 \mu\text{M}$  (Xia and Storm 2005), which is greater than the peak  $\text{Ca}^{2+}$  concentration in our model (3–9  $\mu\text{M}$ ; Fig. 3(b)); however, the activation of the CaM-stimulated enzymes would be possible at this concentration, since the affinity of CaM for  $\text{Ca}^{2+}$  is enhanced in the presence of CaM-binding proteins (Xia and Storm 2005). However, it is not yet understood how the slow intracellular signaling of these agents can detect the difference in  $\text{Ca}^{2+}$  signals and produce STDP. One possibility is that the nonlinear interaction of the  $\text{Ca}^{2+}$ -dependent activity of the kinase and phosphatase (Bhalla and Iyengar 1999; Wang et al. 2005) amplifies the small difference in the initial induction of different signaling pathways (Cavazzini et al. 2005). In particular, the interaction between the cAMP- and calcineurin-mediated pathways (Lisman 1989; Bhalla and Iyengar 1999; Blitzer et al. 1998) might be responsible for regulating the LTD induction, depending on not only the amplitude but also the duration of the  $\text{Ca}^{2+}$  transients in our plasticity model (Eq. (2)) (Mizuno et al. 2001; Yang et al. 1999). Calcium affects adenylate cyclase in a biphasic manner: relatively low  $\text{Ca}^{2+}$  concentrations can stimulate the enzymic activity, while the inhibition of the activity is more difficult and requires higher  $\text{Ca}^{2+}$  concentrations (Piascik et al. 1980). Therefore, it may be possible that during the early phase of the time course of the  $\text{Ca}^{2+}$  transient,  $\text{Ca}^{2+}$  activates adenylate cyclase, which enhances the cAMP-mediated LTD blocking process (Lisman 1989, 1994); however, the prolongation of  $\text{Ca}^{2+}$  elevation might deactivate the cyclase activity again (Piascik et al. 1980). In this case, the calcineurin-mediated LTD process, which is activated by the moderate levels of  $\text{Ca}^{2+}$  increase (Lisman 1989, 1994), overcomes the LTD blocking process by cAMP at a later phase of the  $\text{Ca}^{2+}$  time course, leading to LTD induction for the moderate and prolonged  $\text{Ca}^{2+}$  increase. Furthermore,

such interaction between enzymic activities would also regulate the prolongation of the kinase and phosphatase response even after the  $\text{Ca}^{2+}$  signal is terminated (Bhalla and Iyengar 1999).

#### 4.2 Effects of NMDAR subunit expression on the synaptic plasticity

Our model provides an experimentally verifiable prediction that the NMDAR subunit switch alters the STDP curve such that the areas of the STDP curve under both the LTP and LTD portions decrease, while the ratio of the area under the LTD portion to that under the LTP portion increases (Figs. 3(e) and 4). This prediction is quite robust and does not depend on either the precise parameters in the plasticity model or the action potential waveform (Fig. 4).

There is both direct and indirect evidence that some forms of plasticity may be regulated by the NMDAR expression. Protocols of “pairing” in which presynaptic stimulation is paired with postsynaptic depolarization have shown that the induction of thalamocortical LTP and LTD becomes more difficult when the NMDAR decay accelerates during development (Crair and Malenka 1995; Feldman et al. 1998). These findings are quite similar to our result that the areas of the STDP curve under the LTP and LTD portions decrease (Fig. 4(c and e)). An experiment with thalamocortical synapses has reported that the ability of LTP induction in NR2A knockout mice declines with age, in a manner similar to that observed in wild-type mice, while the NMDAR decay kinetics remains unchanged (Lu et al. 2001). This result may lead to the hypothesis that the developmental decrease in LTP or the critical period plasticity is an NMDAR-independent process (Lu et al. 2001). However, the study by Lu et al. also indicates that the expression levels of NR1 and NR2B subunits are not different between the NR2A knockout and wild-type mice near the end of the critical period (Lu et al. 2001, Fig. 5; see also Sakimura et al. (1995) for similar results). There exists evidence that a significant amount of NR1 protein lacks an NR2 subunit partner (Huh and Wenthold 1999) and the expression of the NR2 subunit rather than that of the NR1 subunit determines the number of functional NMDAR channels (Prybylowski et al. 2002). Therefore, the observation that the NR2A knockout elicits no difference in the NR2B expression (Lu et al. 2001) suggests that the NR2A knockout mice cannot increase the number of NR2B-containing NMDARs and compensate for a loss in NR2A-containing receptors. Therefore, we favor the hypothesis that the total number of functional NMDARs decreases in the NR2A knockout mice near the end of the critical period and the reduction in the total NMDAR current acts to attenuate the synaptically evoked  $\text{Ca}^{2+}$  influx, leading to the reduction in the synaptic potentiation. Although Lu et al.

did not observe the difference in the relative amplitude of the AMPAR and NMDAR currents (AMPA/NMDA) between the NR2A knockout and wild-type mice, another experiment reveals a significant reduction in both the NMDA/AMPA ratio and synaptic potentiation at the hippocampal synapses in the NR2A knockout mice (Sakimura et al. 1995).

Recent experiments have examined the effects of the NR2A- and NR2B-selective antagonists and have shown that selectively blocking the NR2B-containing NMDARs eliminates the LFS-induced LTD but not the HFS-induced LTP, while the inhibition of the NR2A-containing NMDARs prevents the HFS-induced LTP without affecting the LTD production by LFS (Liu et al. 2004; Massey et al. 2004). These findings may be considered to indicate that the activation of NR2A- and NR2B-containing NMDARs is required for the induction of LTP and LTD, respectively (Liu et al. 2004; Massey et al. 2004). This idea leads to the prediction that the developmental increase in the NR2A/B ratio (Quinlan et al. 1999a; Mierau et al. 2004) also increases the LTP/LTD ratio, which is not consistent with our model that indicates an increase in the LTD/LTP ratio (Fig. 4(d and f)). However, the hypothesis that LTP is induced selectively via the NR2A-containing NMDARs is not in agreement with the facts that the thalamocortical LTP becomes difficult to induce when the NMDAR kinetics accelerate (Crair and Malenka 1995) and that the over-expression of NR2B enhances the LTP induction (Tang et al. 1999). Other studies also show contradictory results that indicate that the induction of LTP (Berberich et al. 2005) and LTD (Morishita et al. 2007) does not depend on the activation of specific NR2 subunits in the hippocampus. Furthermore, it may be possible that the frequency- and subunit-dependent regulation of postsynaptic  $\text{Ca}^{2+}$  signals explains in part the distinct effects of the subunit-specific antagonists on LTP and LTD (Erreger et al. 2005). Therefore, we favor the hypothesis that the direction of synaptic plasticity is determined not by the activation of distinct subtypes of NMDARs, but by their coordinated actions for regulating the magnitude and time course of  $\text{Ca}^{2+}$  signals (Morishita et al. 2007).

In rat medial vestibular nuclei (MVN), the HFS protocol induces LTD at very early stage of development, while the probability of inducing LTP increases from the beginning of the second postnatal week and attains the adult level at the end of the third week (Puyal et al. 2003). The LTD process in the MVN is independent of the NMDAR activation; it requires metabotropic glutamate receptor subtype mGluR5 and GABA activity (Puyal et al. 2003), which are beyond the scope of this study. The developmental increase in the ability of LTP induction, which depends on the NMDAR activation (Puyal et al. 2003), is inconsistent with our model. In rat vestibular nuclei, a

significant increase in the NR2C subunit expression is observed within the second and third weeks (Sans et al. 2000). The decay kinetics of the NR1/NR2C NMDARs is as slow as that of the NR1/NR2B receptors (Monyer et al. 1994; Vicini et al. 1998), and the NR1/NR2C channels are less sensitive to the  $Mg^{2+}$  block as compared to the NR1/NR2A and NR1/NR2B channels (Monyer et al. 1994; Kuner and Schoepfer 1996). Therefore, the increase in the NR2C-containing receptors may contribute to enhancing the accumulation of intracellular  $Ca^{2+}$  and increasing the ability of LTP induction. Furthermore, the developmental increase in the mGluR1 expression also plays a role in the facilitation of LTP (Puyal et al. 2003).

#### 4.3 Effects of regulating STDP by NMDAR subunit expression on synaptic weight dynamics

The LIF model simulation has demonstrated that the convergence of synaptic weights into the bimodal distribution is accelerated by switching the STDP learning rule (Fig. 6), as predicted by the Fokker–Planck analysis (Fig. 5). These results suggest that the regulation of STDP by the NMDAR subunit expression can be considered as a biophysical mechanism that promotes rapid and stable growth of immature synapses. The critical role of the subunit switch in this model is to shorten the time required for strengthening weak synapses by STDP with a bias towards LTP at an early phase and induce the bimodal distribution by STDP with a weak bias towards LTD at a later phase (Figs. 5(c) and 6). The timescale of convergence and the impact of the NMDAR subunit switch on the convergence time shown in Fig. 6(g) would be affected by the factors that our model does not incorporate. In particular, the developmental change in the number of synapses and their activity would have a great influence. The LIF model comprises the same number of synapses as that of the third postnatal week and the synaptic input frequency corresponding to the sensory-evoked response for neocortical cells, as mentioned above. However, the number of synapses per neocortical neuron in the neonate is less than one-tenth of that in the third week (Micheva and Beaulieu 1996) and the early phase of synaptic circuit formation can be driven by the spontaneous firing before the onset of sensory-evoked activity (Katz and Shatz 1996; Stern et al. 2001). Therefore, it appears that the pre- and postsynaptic rates of the LIF simulation would be overestimated, particularly in the early phase of the time course of the synaptic weight modification. Since the Fokker–Planck equation (Eq. (13)) suggests that the inverse of the product of the pre- and postsynaptic rates determines the time constant, the inclusion of these effects will greatly expand the timescale of the synaptic weight dynamics during the early phase. This leads to a greater difference in

the time required for strengthening initially weak synapses between the “early” and “late” models (Figs. 5(c) and 6(e)), further increasing the efficacy of the NMDAR subunit switch in accelerating the induction of the bimodal distribution (Fig. 6(g)).

Although the STDP model that induces the bimodal weight distribution makes a significant contribution to the competition and rate stabilization (Kepecs et al. 2002), it is difficult to strengthen weak synapses that cannot evoke frequent postsynaptic firing. The activity-dependent regulation of the NMDAR subunit expression (Quinlan et al. 1999a,b; Carmignoto and Vicini 1992) may function to compensate for this disadvantage of STDP. When the postsynaptic activity is weak, the lower NR2A/B ratio acts to decelerate the NMDAR decay, which primarily increases the possibility of LTP induction and the magnitude of weight change when LTP occurs (Fig. 4(c and e)). Conversely, if the postsynaptic activity becomes sufficiently strong, the higher NR2A/B ratio accelerates the NMDAR decay and decreases the effects of LTP more than those of LTD, which in turn activates the competitive function of STDP (Fig. 5(c)). The activity-dependent expression of NMDARs is particularly important when an undesirable sensory environment, such as dark rearing in a visual system, delays synaptic growth. In this case, the increase in the NR2A/B ratio must be postponed until the environment improves and each synapse is sufficiently strengthened. Otherwise, premature subunit switch may decrease the probability of potentiation and result in greater delay in synaptic growth.

A key assumption in our model is that in order to obtain a bimodal weight distribution, the STDP curve after the subunit switch must satisfy the condition that the area under the LTD portion is slightly larger than that under the LTP portion (Song et al. 2000). This requirement may be automatically satisfied by the  $Ca^{2+}$ -dependent desensitization of the NMDAR channels (Tegner and Kepecs 2002). If the potentiation of the presynaptic inputs increases the postsynaptic activity, frequent discharge would promote the accumulation of intracellular  $Ca^{2+}$  that enters through VGCCs (Helmchen et al. 1996), which is small at very low frequencies (Sabatini et al. 2002). The accumulation of  $Ca^{2+}$  in turn induces the desensitization of the NMDAR channels (Umehiya et al. 2001; Rosenmund et al. 1995). This activity-dependent feedback mechanism may create a balanced state in STDP such that the overall level of depression becomes slightly greater than that of potentiation (Tegner and Kepecs 2002). It should be noted that in our model, STDP before the subunit switch plays a role in rapidly increasing the synaptic weights, and thus, the feedback mechanism is required only after the subunit switch. This can explain the experimental findings that  $Ca^{2+}$ -dependent inactivation is observed in NR1/NR2A receptors but not in

NR1/NR2B receptors (Umemiya et al. 2001; Krupp et al. 1996). It would be of interest to study how early synapses are organized when the subunit-specific  $\text{Ca}^{2+}$ -dependent desensitization of NMDARs is introduced in combination with a change in the decay kinetics considered here.

#### 4.4 Effects of NMDAR subunit expression on the development of topographic maps

Our model also predicts that the NMDAR subunit expression regulates the development of topographic maps. Let us consider how the subunit switch affects the network in Fig. 7(a) (lower panel), which represents the projections from thalamic relay neurons (open circles) to recurrently interconnected cortical neurons (colored circles) (Song and Abbott 2001). The activity of each thalamic relay cell may, for example, represent the location of a tactile stimulation on the skin or the orientation of a visual image on the retina. In very early development, a coarse topographic map is generated in an activity-independent manner (Goodman and Shatz 1993) (Fig. 7(a), lower panel). Since the initial synaptic connections are very weak and overlapping (Issac et al. 1997; Goodman and Shatz 1993), the firing activity of each cortical cell is weak and less-selective to sensory inputs, as shown by the response tuning curve for each cortical neuron (Fig. 7(a), upper panel). A small NR2A/B ratio and the resulting slower NMDAR kinetics strengthen all the presynaptic connections to a given postsynaptic cell (Figs. 5(c), 6(c), and 7(b) (lower panel)); therefore, it is difficult to increase the input selectivity of the cortical cells. The resulting response tuning curves have higher peak amplitude, while each curve remains broad (Fig. 7(b), upper panel). On the other hand, a large NR2A/B ratio accelerates the NMDAR decay and induces competition among the presynaptic inputs (Figs. 5(c) and 6(d)). This contributes to refining the topographic map (Fig. 7(c), lower panel), increasing the input selectivity, and making sharp response tuning curves (Fig. 7(c), upper panel), as shown by the model of Song and Abbott (2001). In cases where the NMDAR subunit switch occurs during development, the synaptic connections are at first strengthened by the smaller NR2A/B ratio and then refined by the increase in the NR2A/B ratio (Fig. 7, curved arrow). Therefore, we can predict that the input selectivity of neurons is significantly increased during a period in which the NMDAR subunit composition changes. This prediction is experimentally verifiable by simultaneously measuring the developmental change in the selectivity of neurons for some aspects of inputs with the NMDAR decay time constant or the expression levels of different NR2 subunits. Furthermore, the discussion here suggests that the input selectivity of neurons can be regulated via transgenic manipulations. For example, the overexpression of the NR2B subunit, which

decelerates the NMDAR decay particularly in later developmental stages (Tang et al. 1999), will reduce the input selectivity of neurons at adulthood. The region-specific knockout of NMDARs (McHugh et al. 1996) will severely impair the selectivity to specific aspects of the input. The knockout of the NR2A subunit may also impair the input selectivity to some degree by the decrease in the total NMDAR current (Sakimura et al. 1995), as discussed above. The topographic maps with neurons with adequate levels of input selectivity would be important to permit efficient communication between appropriate sets of neurons (Kaas 1997). Therefore, we consider that increasing the rate of induction of the synaptic competition through the NMDAR subunit switch (Fig. 6(g)) is required for

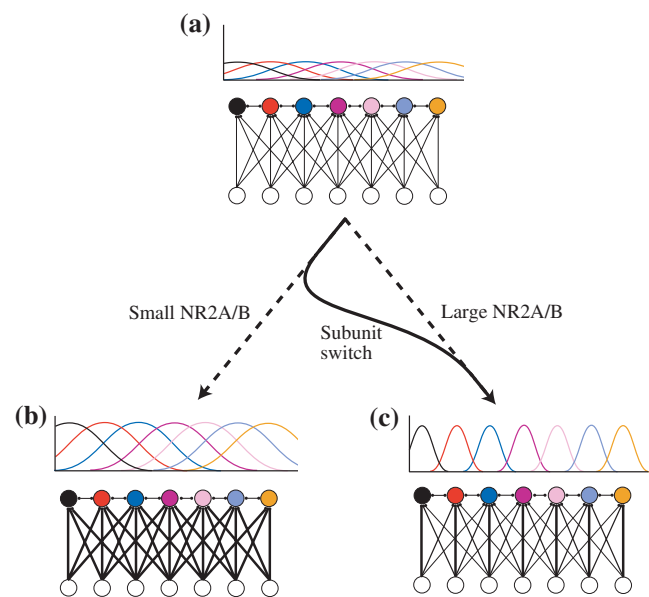


**Fig. 7** Predicted effects of the NMDAR subunit expression on the development of topographic maps. The *lower panel* in (a–c): the synaptic circuits that represent the projections from the thalamic relay neurons (*open circles*) to the cortical neurons (*colored circles*). The thalamic relay neurons are spatially distributed such that their positions reflect their preferred stimuli (e.g., orientation angle of a visual image). The strength of feedforward connections are denoted by the *line thickness*. The upper panel in (a–c): the neural response tuning curves for the cortical neurons (e.g., firing activity of a neuron in the primary visual cortex vs. orientation angle of the visual image). The color of each line corresponds to that of the cortical neuron. (a) In very early development, weak and coarse topographic connections are formed by activity-independent mechanisms (*lower panel*). In this stage, the firing activity of neurons is low and their tuning curves are broad (*upper panel*). (b) A small NR2A/B ratio strengthens all synaptic connections (*lower panel*); therefore, the response tuning curves remain broad (*upper panel*). (c) A large NR2A/B ratio induces competition among the presynaptic inputs and refines the topographic map (*lower panel*), producing sharp tuning curves (*upper panel*). The *curved arrow*: when the NMDAR subunit switch occurs, synaptic connections are strengthened initially with the smaller NR2A/B ratio and the topographic pattern is then refined by the larger NR2A/B ratio. This contributes to developing the refined topographic maps quite rapidly

developing the input selectivity of neurons and producing refined topographic connections in earlier stages.

### Appendix A: Derivation of Eqs. (13–15)

As shown in van Rossum et al. (2000), synaptic weight distribution  $P(w)$  obeys

$$\frac{1}{f_{\text{pre}}} \frac{\partial P(w, t)}{\partial t} = -\frac{\partial}{\partial w} [r_1(w)P(w, t)] + \frac{1}{2} \frac{\partial^2}{\partial w^2} [r_2(w)P(w, t)], \quad (16)$$

$$r_1(w) = A_+ p_p - A_- p_d, \quad (17)$$

$$r_2(w) = A_+^2 p_p + A_-^2 p_d, \quad (18)$$

where  $p_p$  and  $p_d$  denote the probability that LTP and LTD occur by the presynaptic event, respectively. By the same assumptions as van Rossum et al., we obtain the following relations:  $p_d = f_{\text{post}t-}$  and  $p_p = p_d(t_+/t_-)(1+w/W_{\text{tot}})$ . If we substitute these equations into Eqs. (17) and (18), and set  $A(w) = r_1(w)/f_{\text{post}}$  and  $B(w) = r_2(w)/f_{\text{post}}$ , then Eqs. (16–18) can be rewritten as Eqs. (13–15).

**Acknowledgement** This study is partially supported by the Grant-in-Aid for Scientific Research (KAKENHI (19700281), Young Scientists (B)) from the Ministry of Education, Culture, Sports, Science and Technology of Japan.

### References

- Abarbanel, H. D. I., Gibb, L., Huerta, R., & Rabinovich, M. I. (2003). Biophysical model of synaptic plasticity dynamics. *Biological Cybernetics*, *89*, 214–226.
- Abbott, L. F., & Nelson, S. B. (2000). Synaptic plasticity: Taming the beast. *Nature Neuroscience*, *3*(Suppl), 1178–1183.
- Ahmed, B., Anderson, J. C., Douglas, R. J., Martin, K. A. C., & Whitteridge, D. (1998). Estimates of the net excitatory currents evoked by visual stimulation of identified neurons in cat visual cortex. *Cerebral Cortex*, *8*, 462–476.
- Artola, A., & Singer, W. (1993). Long-term depression of excitatory synaptic transmission and its relationship to long-term potentiation. *Trends in Neurosciences*, *16*, 480–487.
- Bear M. F., Cooper L. N., & Ebner F. F. (1987). A physiological basis for a theory of synapse modification. *Science*, *237*, 42–48.
- Berberich, S., Punnakkal, P., Jensen, V., Pawlak, V., Seeburg, P. H., Hvalby, O., et al. (2005). Lack of NMDA receptor subtype selectivity for hippocampal long-term potentiation. *Journal of Neuroscience*, *25*, 6907–6910.
- Bernander, O., Douglas, R. J., Martin, K. A. C., & Koch, C. (1991). Synaptic background activity influences spatiotemporal integration in single pyramidal cells. *Proceedings of the National Academy of Sciences of the United States of America*, *88*, 11569–11573.
- Bhalla, U. S., & Iyengar, R. (1999). Emergent properties of networks of biological signaling pathways. *Science*, *283*, 381–387.
- Bi, G. Q., & Poo, M. M. (1998). Synaptic modifications in cultured hippocampal neurons: Dependence on spike timing, synaptic strength, and postsynaptic cell type. *Journal of Neuroscience*, *18*, 10464–10472.
- Bi, G. Q., & Rubin, J. (2005). Timing in synaptic plasticity: From detection to integration. *Trends in Neurosciences*, *28*, 222–228.
- Blitzer, R. D., Connor, J. H., Brown, G. P., Wong, T., Shenolikar, S., & Iyengar, R., et al. (1998). Gating of CaMKII by cAMP-regulated protein phosphatase activity during LTP. *Science*, *280*, 1940–1943.
- Bush, P. C., & Sejnowski, T. J. (1993). Reduced compartmental models of neocortical pyramidal cells. *Journal of Neuroscience Methods*, *46*, 159–166.
- Callaway, J. C., & Ross, W. N. (1995). Frequency-dependent propagation of sodium action potentials in dendrites of hippocampal CA1 pyramidal neurons. *Journal of Neurophysiology*, *74*, 1395–1403.
- Carmignoto, G., & Vicini, S. (1992). Activity-dependent decrease in NMDA receptor responses during development of the visual cortex. *Science*, *258*, 1007–1011.
- Cavazzini, M., Bliss, T., & Emptage, N. (2005).  $\text{Ca}^{2+}$  and synaptic plasticity. *Cell Calcium*, *38*, 355–367.
- Crair, M. C., & Malenka, R. C. (1995). A critical period for long-term potentiation at thalamocortical synapses. *Nature*, *375*, 325–328.
- Daw, N. W., Gordon, B., Fox, K. D., Flavin, H. J., Kirsch, J. D., Beaver, C. J., et al. (1999). Injection of MK-801 affects ocular dominance shifts more than visual activity. *Journal of Neurophysiology*, *81*, 204–215.
- Debanne, D., Gähwiler, B. H., & Thompson, S. M. (1998). Long-term synaptic plasticity between pairs of individual CA3 pyramidal cells in rat hippocampal slice cultures. *Journal of Physiology (London)*, *507.1*, 237–247.
- Dumas, T. C. (2005). Developmental regulation of cognitive abilities: Modified composition of a molecular switch turns on associative learning. *Progress in Neurobiology*, *76*, 189–211.
- Erreger, K., Dravid, S. M., Banke, T. G., Wyllie, D. J. A., & Traynelis, S. F. (2005). Subunit-specific gating controls rat NR1/NR2A and NR1/NR2B NMDA channel kinetics and synaptic signalling profiles. *Journal of Physiology (London)*, *563.2*, 345–358.
- Fagiolini, M., Pizzorusso, T., Berardi, N., Domenici, L., & Maffei, L. (1994). Functional postnatal development of the rat primary visual cortex and the role of visual experience: Dark rearing and monocular deprivation. *Vision Research*, *34*, 709–720.
- Feldman, D. E. (2000). Timing-based LTP and LTD at vertical inputs to layer II/III pyramidal cells in rat barrel cortex. *Neuron*, *27*, 45–56.
- Feldman, D. E., Nicoll, R. A., Malenka, R. C., & Isaac, J. T. R. (1998). Long-term depression at thalamocortical synapses in developing rat somatosensory cortex. *Neuron*, *21*, 347–357.
- Flint, A. C., Maisch, U. S., Weishaupt, J. H., Kriegstein, A. R., & Monyer, H. (1997). NR2A subunit expression shortens NMDA receptor synaptic currents in developing neocortex. *Journal of Neuroscience*, *17*, 2469–2476.
- Froemke, R. C., Poo, M. M., & Dan, Y. (2005). Spike-timing-dependent synaptic plasticity depends on dendritic location. *Nature*, *434*, 221–225.
- Gerstner, W., & Kistler, W. M. (2002). *Spiking neuron models: Single neurons, populations, plasticity*. Cambridge: Cambridge University Press.
- Goodman, C. S., & Shatz, C. J. (1993). Developmental mechanisms that generate precise patterns of neuronal connectivity. *Cell* *72* / *Neuron*, *10*(Suppl.), 77–98.

- Harris, K. M., Jansen, F. E., & Tsao, B. (1992). Three-dimensional structure of dendritic spines and synapses in rat hippocampus (CA1) at postnatal day 15 and adult ages: Implications for the maturation of synaptic physiology and long-term potentiation. *Journal of Neuroscience*, *12*, 2685–2705.
- Helmchen, F., Imoto, K., & Sakmann, B. (1996).  $\text{Ca}^{2+}$  buffering and action potential-evoked  $\text{Ca}^{2+}$  signaling in dendrites of pyramidal neurons. *Biophysical Journal*, *70*, 1069–1081.
- Hessler, N. A., Shirke, A. M., & Mallnow, R. (1993). The probability of transmitter release at a mammalian central synapse. *Nature*, *366*, 569–572.
- Holmes. (2000). Models of calmodulin trapping and CaM kinase II activation in a dendritic spine. *Journal of Computational Neuroscience*, *8*, 65–85.
- Huh, K. H., & Wenthold, R. J. (1999). Turnover analysis of glutamate receptors identifies a rapidly degraded pool of the N-Methyl-D-aspartate receptor subunit, NR1, in cultured cerebellar granule cells. *Journal of Biological Chemistry*, *274*, 151–157.
- Iannella, N., & Tanaka, S. (2006). Synaptic efficacy cluster formation across the dendrite via STDP. *Neuroscience Letters*, *403*, 24–29.
- Issac, J. T. R., Crair, M. C., Nicoll, R. A., & Malenka, R. C. (1997). Silent synapses during development of thalamocortical inputs. *Neuron*, *18*, 269–280.
- Jahr, C. E., & Stevens, C. F. (1990a). Quantitative description of NMDA receptor-channel kinetic behavior. *Journal of Neuroscience*, *10*, 1830–1837.
- Jahr, C. E., & Stevens, C. F. (1990b). Voltage dependence of NMDA-activated macroscopic conductances predicted by single-channel kinetics. *Journal of Neuroscience*, *10*, 3178–3182.
- Kaas, J. H. (1997). Topographic maps are fundamental to sensory processing. *Brain Research Bulletin*, *44*, 107–112.
- Karmarkar, U. R., & Buonomano, D. V. (2002). A model of spike-timing dependent plasticity: One or two coincidence detectors? *Journal of Neurophysiology*, *88*, 507–513.
- Karmarkar, U. R., Najarian, M. T., & Buonomano, D. V. (2002). Mechanisms and significance of spike-timing dependent plasticity. *Biological Cybernetics*, *87*, 373–382.
- Kato, N., & Yoshimura, H. (1993). Reduced  $\text{Mg}^{2+}$  block of N-methyl-D-aspartate receptor-mediated synaptic potentials in developing visual cortex. *Proceedings of the National Academy of Sciences of the United States of America*, *90*, 7114–7118.
- Katz, L. C., & Shatz, C. J. (1996). Synaptic activity and the construction of cortical circuits. *Science*, *274*, 1133–1138.
- Kepecs, A., van Rossum, M. C. W., Song, S., & Tegner, J. (2002). Spike-timing-dependent plasticity: Common themes and divergent vistas. *Biological Cybernetics*, *87*, 446–458.
- Kirson, E. D., Schirra, C., Konnerth, A., & Yaari, Y. (1999). Early postnatal switch in magnesium sensitivity of NMDA receptors in rat CA1 pyramidal cells. *Journal of Physiology (London)*, *521.1*, 99–111.
- Kitajima, T., & Hara, K. (2000). A generalized Hebbian rule for activity-dependent synaptic modifications. *Neural Networks*, *13*, 445–454.
- Koch, C. (1999). *Biophysics of computation. Information processing in single neurons*. New York: Oxford University Press.
- Kovalchuk, Y., Eilers, J., Lisman, J., & Konnerth, A. (2000). NMDA receptor-mediated subthreshold  $\text{Ca}^{2+}$  signals in spines of hippocampal neurons. *Journal of Neuroscience*, *20*, 1791–1799.
- Krupp, J. J., Vissel, B., Heinemann, S. F., & Westbrook, G. L. (1996). Calcium-dependent inactivation of recombinant N-methyl-D-aspartate receptors is NR2 subunit specific. *Molecular Pharmacology*, *50*, 1680–1688.
- Kuner, T., & Schoepfer, R. (1996). Multiple structural elements determine subunit specificity of  $\text{Mg}^{2+}$  block in NMDA receptor channels. *Journal of Neuroscience*, *16*, 3549–3558.
- Lancaster, B., & Zucker, R. S. (1994). Photolytic manipulation of  $\text{Ca}^{2+}$  and the time course of slow,  $\text{Ca}^{2+}$ -activated  $\text{K}^{+}$  current in rat hippocampal neurons. *Journal of Physiology (London)*, *475.2*, 229–239.
- Lisman, J. (1989). A mechanism for the Hebb and the anti-Hebb processes underlying learning and memory. *Proceedings of the National Academy of Sciences of the United States of America*, *86*, 9574–9578.
- Lisman, J. (1994). The CaM kinase II hypothesis for the storage of synaptic memory. *Trends in Neurosciences*, *17*, 406–412.
- Lisman, J. E., & Zhabotinsky, A. M. (2001). A model of synaptic memory: A CaMKII/PP1 switch that potentiates transmission by organizing an AMPA receptor anchoring assembly. *Neuron*, *31*, 191–201.
- Liu, L., Wong, T. P., Pozza, M. F., Lingenhoehl, K., Wang, Y., Sheng, M., et al. (2004). Role of NMDA receptor subtypes in governing the direction of hippocampal synaptic plasticity. *Science*, *304*, 1021–1024.
- Liu, Y. H., & Wang, X. J. (2001). Spike-frequency adaptation of a generalized leaky integrate-and-fire model neuron. *Journal of Computational Neuroscience*, *10*, 25–45.
- Llinas, R. R. (1988). The intrinsic electrophysiological properties of mammalian neurons: Insights into central nervous system function. *Science*, *242*, 1654–1664.
- Lu, H. C., Gonzalez, E., & Crair, M. C. (2001). Barrel cortex critical period plasticity is independent of changes in NMDA receptor subunit composition. *Neuron*, *32*, 619–634.
- Mainen, Z. F., & Sejnowski, T. J. (1996). Influence of dendritic structure on firing pattern in model neocortical neurons. *Nature*, *382*, 363–366.
- Markram, H., Lubke, J., Frotscher, M., & Sakmann, B. (1997). Regulation of synaptic efficacy by coincidence of postsynaptic APs and EPSPs. *Science*, *275*, 213–215.
- Massey, P. V., Johnson, B. E., Moul, P. R., Auberson, Y. P., Brown, M. W., Molnar, E., et al. (2004). Differential roles of NR2A and NR2B-containing NMDA receptors in cortical long-term potentiation and long-term depression. *Journal of Neuroscience*, *24*, 7821–7828.
- McCormick, D. A., Connors, B. W., Lighthall, J. W., & Prince, D. A. (1985). Comparative electrophysiology of pyramidal and sparsely spiny stellate neurons of the neocortex. *Journal of Neurophysiology*, *54*, 782–806.
- McHugh, T. J., Blum, K. I., Tsien, J. Z., Tonegawa, S., & Wilson, M. A. (1996). Impaired hippocampal representation of space in CA1-specific NMDAR1 knockout mice. *Cell*, *87*, 1339–1349.
- Micheva, K. D., & Beaulieu, C. (1996). Quantitative aspects of synaptogenesis in the rat barrel field cortex with special reference to GABA circuitry. *Journal of Comparative Neurology*, *373*, 340–354.
- Mierau, S. B., Meredith, R. M., Upton, A. L., & Paulsen, O. (2004). Dissociation of experience-dependent and -independent changes in excitatory synaptic transmission during development of barrel cortex. *Proceedings of the National Academy of Sciences of the United States of America*, *101*, 15518–15523.
- Mizuno, T., Kanazawa, I., & Sakurai, M. (2001). Differential induction of LTP and LTD is not determined solely by instantaneous calcium concentration: An essential involvement of a temporal factor. *European Journal of Neuroscience*, *14*, 701–708.
- Monyer, H., Burnashev, N., Laurie, D. J., Sakmann, B., & Seeburg, P. H. (1994). Developmental and regional expression in the rat brain and functional properties of four NMDA receptors. *Neuron*, *12*, 529–540.
- Morishita, W., Lu, W., Smith, G. B., Nicoll, R. A., Bear, M. F., & Malenka, R. C. (2007). Activation of NR2B-containing NMDA receptors is not required for NMDA receptor-dependent long-term depression. *Neuropharmacology*, *52*, 71–76.

- Nishiyama, M., Hong, K., Mikoshiba, K., Poo, M. M., & Kato, K. (2000). Calcium stores regulate the polarity and input specificity of synaptic modification. *Nature*, *408*, 584–588.
- Philpot, B. D., Sekhar, A. K., Shouval, H. Z., & Bear, M. F. (2001). Visual experience and deprivation bidirectionally modify the composition and function of NMDA receptors in visual cortex. *Neuron*, *29*, 157–169.
- Piascik, M. T., Wisler, P. L., Johnson, C. L., & Potter, J. D. (1980).  $Ca^{2+}$ -dependent regulation of guinea pig brain adenylate cyclase. *Journal of Biological Chemistry*, *255*, 4176–4181.
- Press, W. H., Flannery, B. P., Teukolsky, S. A., & Vetterling, W. T. (1988). *Numerical recipes in C*. Cambridge: Cambridge University Press.
- Prybylowski, K., Fu, Z., Losi, G., Hawkins, L. M., Luo, J., Chang, K., et al. (2002). Relationship between availability of NMDA receptor subunits and their expression at the synapse. *Journal of Neuroscience*, *22*, 8902–8910.
- Puyal, J., Grassi, S., Dieni, C., Frondaroli, A., Demêmes, D., Raymond, J., et al. (2003). Developmental shift from long-term depression to long-term potentiation in the rat medial vestibular nuclei: Role of group I metabotropic glutamate receptors. *Journal of Physiology (London)*, *553*, 427–443.
- Quinlan, E. M., Olstein, D. H., & Bear, M. F. (1999a). Bidirectional, experience-dependent regulation of N-methyl-D-aspartate receptor subunit composition in the rat visual cortex during postnatal development. *Proceedings of the National Academy of Sciences of the United States of America*, *96*, 12876–12880.
- Quinlan, E. M., Philpot, B. D., Haganir, R. L., & Bear, M. F. (1999b). Rapid, experience-dependent expression of synaptic NMDA receptors in visual cortex in vivo. *Nature Neuroscience*, *2*, 352–357.
- Rema, V., Armstrong-James, M., & Ebner, F. F. (1998). Experience-dependent plasticity of adult rat S1 cortex requires local NMDA receptor activation. *Journal of Neuroscience*, *18*, 10196–10206.
- Risken, H. (1989). *The Fokker–Planck equation: Methods of solution and applications* (2nd edn.). Berlin: Springer.
- Rosenmund, C., Feltz, A., & Westbrook, G. L. (1995). Calcium-dependent inactivation of synaptic NMDA receptors in hippocampal neurons. *Journal of Neurophysiology*, *73*, 427–430.
- Rubin, J., Lee, D. D., & Sompolinsky, H. (2001). Equilibrium properties of temporally asymmetric Hebbian plasticity. *Physical Review Letters*, *86*, 364–367.
- Rubin, J. E., Gerkin, R. C., Bi, G. Q., & Chow, C. C. (2005). Calcium time course as a signal for spike-timing-dependent plasticity. *Journal of Neurophysiology*, *93*, 2600–2613.
- Rumsey, C. C., & Abbott, L. F. (2006). Synaptic democracy in active dendrites. *Journal of Neurophysiology*, *96*, 2307–2318.
- Sabatini, B. L., Maravall, M., & Svoboda, K. (2001).  $Ca^{2+}$  signaling in dendritic spines. *Current Opinion in Neurobiology*, *11*, 349–356.
- Sabatini, B. L., Oertner, T. G., & Svoboda, K. (2002). The life cycle of  $Ca^{2+}$  ions in dendritic spines. *Neuron*, *33*, 439–452.
- Sah, P., & Bekkers, J. M. (1996). Apical dendritic location of slow afterhyperpolarization current in hippocampal pyramidal neurons: Implications for the integration of long-term potentiation. *Journal of Neuroscience*, *16*, 4537–4542.
- Sakimura, K., Kutsuwada, T., Ito, I., Manabe, T., Takayama, C., Kushiya, E., et al. (1995). Reduced hippocampal LTP and spatial learning in mice lacking NMDA receptor  $\epsilon 1$  subunit. *Nature*, *373*, 151–155.
- Sans, N. A., Montcouquiol, M. E., & Raymond, J. (2000). Postnatal developmental changes in AMPA and NMDA receptors in the rat vestibular nuclei. *Developmental Brain Research*, *123*, 41–52.
- Schiller, J., Helmchen, F., & Sakmann, B. (1995). Spatial profile of dendritic calcium transients evoked by action potentials in rat neocortical pyramidal neurons. *Journal of Physiology (London)*, *487*, 583–600.
- Schneggenburger, R. (1996). Simultaneous measurement of  $Ca^{2+}$  influx and reversal potentials in recombinant N-methyl-D-aspartate receptor channels. *Biophysical Journal*, *70*, 2165–2174.
- Schneggenburger, R., Zhou, Z., Konnerth, A., & Neher, E. (1993). Fractional contribution of calcium to the cation current through glutamate receptor channels. *Neuron*, *11*, 133–143.
- Sheng, M., Cummings, J., Roldan, L. A., Jan, Y. N., & Jan, L. Y. (1994). Changing subunit composition of heteromeric NMDA receptors during development of rat cortex. *Nature*, *368*, 144–147.
- Shi, J., Aamodt, S. M., & Constantine-Paton, M. (1997). Temporal correlations between functional and molecular changes in NMDA receptors and GABA neurotransmission in the superior colliculus. *Journal of Neuroscience*, *17*, 6264–6276.
- Shouval, H. Z., Bear, M. F., & Cooper, L. N. (2002). A unified model of NMDA receptor-dependent bidirectional synaptic plasticity. *Proceedings of the National Academy of Sciences of the United States of America*, *99*, 10831–10836.
- Shouval, H. Z., & Kalantzis, G. (2005). Stochastic properties of synaptic transmission affect the shape of spike time-dependent plasticity curves. *Journal of Neurophysiology*, *93*, 1069–1073.
- Simons, D. J. (1978). Response properties of vibrissa units in rat SI somatosensory neocortex. *Journal of Neurophysiology*, *41*, 798–820.
- Simons, D. J., & Carvell, G. E. (1989). Thalamocortical response transformation in the rat vibrissa/barrel system. *Journal of Neurophysiology*, *61*, 311–330.
- Song, S., & Abbott, L. F. (2001). Cortical development and remapping through spike timing-dependent plasticity. *Neuron*, *32*, 339–350.
- Song, S., Miller, K. D., & Abbott, L. F. (2000). Competitive Hebbian learning through spike-timing-dependent synaptic plasticity. *Nature Neuroscience*, *3*, 919–926.
- Steigerwald, F., Schulz, T. W., Schenker, L. T., Kennedy, M. B., Seeburg, P. H., & Köhr, G. (2000). C-terminal truncation of NR2A subunits impairs synaptic but not extrasynaptic localization of NMDA receptors. *Journal of Neuroscience*, *20*, 4573–4581.
- Stephenson, F. A. (2001). Subunit characterization of NMDA receptors. *Current Drug Targets*, *2*, 233–239.
- Stern, E. A., Maravall, M., & Svoboda, K. (2001). Rapid development and plasticity of layer 2/3 maps in rat barrel cortex in vivo. *Neuron*, *31*, 305–315.
- Svoboda, K., Denk, W., Kleinfeld, D., & Tank, D. W. (1997). In vivo dendritic calcium dynamics in neocortical pyramidal neurons. *Nature*, *385*, 161–165.
- Tang, Y. P., Shimizu, E., Dube, G. R., Rampon, C., Kerchner, G. A., Zhuo, M., et al. (1999). Genetic enhancement of learning and memory in mice. *Nature*, *401*, 63–69.
- Tateno, T., Harsch, A., & Robinson, H. P. C. (2004). Threshold firing frequency-current relationships of neurons in rat somatosensory cortex: Type 1 and type 2 dynamics. *Journal of Neurophysiology*, *92*, 2283–2294.
- Tegner, J., & Kepecs, A. (2002). Why neuronal dynamics should control synaptic learning rules. In T. G. Dietterich, S. Becker, & Z. Ghahramani (Eds.), *Advances in Neural Information Processing Systems 14*. Cambridge: MIT Press.
- Togashi, K., Kitajima, T., Aihara, T., Hong, K., Poo, M., & Nishiyama, M. (2003). Gating of activity-dependent long-term depression by GABAergic activity in the hippocampus. *Society for Neuroscience*, *123*, 4(Abtract).
- Troyer, T. W., & Miller, K. D. (1997). Physiological gain leads to high ISI variability in a simple model of a cortical regular spiking cell. *Neural Computation*, *9*, 971–983.

- Umekiya, M., Chen, N., Raymond, L. A., & Murphy, T. H. (2001). A calcium-dependent feedback mechanism participates in shaping single NMDA miniature EPSCs. *Journal of Neuroscience*, *21*, 1–9.
- Van Rossum, M. C. W., Bi, G. Q., & Turrigiano, G. G. (2000). Stable Hebbian learning from spike timing-dependent plasticity. *Journal of Neuroscience*, *20*, 8812–8821.
- Vicini, S., Wang, J. F., Li, J. H., Zhu, W. J., Wang, Y. H., Luo, J. H., et al. (1998). Functional and pharmacological differences between recombinant N-methyl-D-aspartate receptors. *Journal of Neurophysiology*, *79*, 555–566.
- Wang, H. X., Gerkin, R. C., Nauen, D. W., & Bi, G. Q. (2005). Coactivation and timing-dependent integration of synaptic potentiation and depression. *Nature Neuroscience*, *8*, 187–193.
- Xia, Z., & Storm, D. R. (2005). The role of calmodulin as a signal integrator for synaptic plasticity. *Nature Reviews. Neuroscience*, *6*, 267–276.
- Yang, S. N., Tang, Y. G., & Zucker, R. S. (1999). Selective induction of LTP and LTD by postsynaptic  $[Ca^{2+}]_i$  elevation. *Journal of Neurophysiology*, *81*, 781–787.
- Zador, A., Koch, C., & Brown, T. H. (1990). Biophysical model of a Hebbian synapse. *Proceedings of the National Academy of Sciences of the United States of America*, *87*, 6718–6722.
- Zhabotinsky. (2000). Bistability in the  $Ca^{2+}$ /calmodulin-dependent protein kinase-phosphatase system. *Biophysical Journal*, *79*, 2211–2221.
- Zhang, L. I., Tao, H. W., Holt, C. E., Harris, W. A., & Poo, M. M. (1998). A critical window for cooperation and competition among developing retinotectal synapses. *Nature*, *395*, 37–44.